J. Fluid Mech. (2014), *vol.* 758, *pp.* 238–286. © Cambridge University Press 2014
doi:10.1017/jfm.2014.499

On the disturbance evolution downstream of a cylindrical roughness element

B. Plogmann[1,†], W. Würz[1] and E. Krämer[1]

[1]Institute of Aerodynamics and Gas Dynamics, University of Stuttgart, Pfaffenwaldring 21, 70569 Stuttgart, Germany

(Received 14 January 2014; revised 1 July 2014; accepted 22 August 2014; first published online 8 October 2014)

Roughness-induced transition is one of the main parameters contributing to performance loss of airfoils. Within this paper, the disturbance evolution downstream of a single, cylindrical roughness element, which is placed in a laminar boundary layer in an airfoil leading edge region, is investigated. The experiments focus on medium height roughness elements with respect to the local boundary layer displacement thickness. Hence, transition is not directly tripped at the roughness element. The roughness diameter is comparable to the streamwise wavelength of the most amplified (linear) disturbance eigenmodes. The vortical structures observed downstream of the roughness are in agreement with previous findings in the literature. In the near roughness wake, a distinct growth of high-frequency (fundamental) modes, that is modes with a high n-factor at the roughness location, is observed. In the far roughness wake, these fundamental modes recover linear stability characteristics due to a possible relaxation of the mean flow. However, an interaction of particularly two-dimensional fundamental modes and by the roughness interference excited oblique fundamental modes results in an excitation of subharmonic type, low-frequency combination modes, which are associated with a phase-locked interaction mechanism. Depending on the initial growth of the fundamental modes in the near wake, the low-frequency modes can experience a nonlinear growth in the far roughness wake and, thereby, trip turbulence. The fundamental mode growth rate in the near wake in turn is a weak function of the disturbance frequency and of the pressure gradient, whereas it is decisively increasing with the roughness height, that is with the mean flow distortion caused by the roughness.

Key words: boundary layer stability, nonlinear instability, transition to turbulence

1. Introduction

Since the development of the first airfoils with long laminar run, the influence of surface roughness on the laminar to turbulent transition process has been of particular interest (Jacobs 1939). The first wind tunnel experiments have, therefore, already been conducted in the early 1940s by Tani & Hama (1940) and Fage (1943). At first, mainly the influence of the roughness dimensions on the transition location has been investigated resulting in criteria for the transition Reynolds number with

† Email address for correspondence: plogmann@iag.uni-stuttgart.de

https://doi.org/10.1017/jfm.2014.499 Published online by Cambridge University Press

respect to simple shape parameters of the roughness. In general, three different types of roughness elements can be distinguished based on their shape: two-dimensional roughness elements, isolated three-dimensional roughness elements (Tani 1961) and distributed three-dimensional elements (von Doenhoff & Braslow 1961). The latter can either be regularly spaced (also referred to as roughness array) or be composed of randomly distributed roughness elements.

For an isolated three-dimensional roughness element immersed in a two-dimensional laminar boundary layer, first flow visualizations by Gregory & Walker (1956) revealed a wedge-shaped region, in which boundary layer transition was seen to occur. The visualization of the arising vortical structures were complemented by the work of Mochizuki (1961*a*,*b*). In contrast, the flow structures developing in the wake of a two-dimensional roughness element are considerably different. Klebanoff & Tidstrom (1972) attributed transition to a strong mean flow distortion induced by the roughness element. Therefore, transition aft of a two-dimensional roughness element moves rather gradually towards the roughness element with increasing roughness Reynolds number R_h ($R_h = u_h h/\nu$ with u_h being the velocity at the roughness height, h the roughness height and ν the kinematic viscosity). According to Morkovin (1990), the characteristic feature is a long separation bubble in the roughness wake. Correspondingly, a significant amplification of disturbances, introduced into the boundary layer upstream of the roughness element with the help of a vibrating ribbon, could be shown by Dovgal & Kozlov (1990) in the distorted mean flow region. In contrast, for a three-dimensional roughness element transition approaches the roughness position rapidly, as the critical roughness Reynolds number $R_{h,crit}$ is exceeded, whereas boundary layer transition is not considerably affected below $R_{h,crit}$ (Dryden 1953; Tani 1969). Numerically, the mean flow stability behaviour aft of the roughness was studied using the concept of interactive boundary layers (Nayfeh, Ragab & Al-Maaitah 1988; Cebeci & Egan 1989; Masad & Lyer 1994). The work of Masad & Lyer (1994) accounted for various flow parameters such as height, length, location and shape of the roughness and unit Reynolds number. An evaluation of the n-factors based on the transition location was performed and seen to be in good agreement with wind tunnel and free flight experiments. The numerical results by Nayfeh *et al.* (1988) were correlated with previous experiments leading to n-factors of 7–10. More recently, the effect of forward and backward facing steps was modelled with a variable n-factor method showing a larger n-factor reduction for a backward facing step (Crouch, Kosorygi & Ng 2006). Moreover, this study reveals higher n-factors for a favourable compared with an adverse pressure gradient boundary layer.

In the early experiments the roughness heights were often large (of the order of one displacement thickness) and, therefore, flow separation downstream of the roughness element is the key parameter affecting boundary layer transition. However, since the flow phenomena alter significantly with the roughness height a further separation into three different categories is worthwhile, in particular, low (i), medium (ii) and high (iii) roughness heights.

For low roughness heights (i), base flow velocity variations caused by the roughness element are very small. Nevertheless, such small-scale velocity variations can result in an energy transfer from large-scale free-stream disturbances to boundary layer instability modes (Tollmien–Schlichting (TS) waves). This receptivity process was experimentally shown by Aizin & Polyakov (1979) for two-dimensional roughness elements and later on confirmed by Ruban (1984) and Goldstein (1985) using the triple deck analysis. According to Saric, Hoos & Radezsky (1991), the receptivity

https://doi.org/10.1017/jfm.2014.499 Published online by Cambridge University Press

process is very sensitive to the disturbance frequency and the roughness height. A linear relationship between roughness height and generated TS wave amplitude is only present below a certain threshold value for the roughness Reynolds number, which is near $R_h = 5$. In the following, this receptivity process was also addressed for three-dimensional roughness elements (Choudhari & Kerschen 1990; Tadjfar & Bodonyi 1992) interacting with different types of free-stream disturbances. Würz *et al.* (2003) found an increased receptivity towards external, in that case acoustical, disturbances for non-zero spanwise wavenumbers of the roughness element in their experimental and numerical investigations. Further details on the receptivity process are reviewed by Kachanov (2000) and Saric, Reed & Kerschen (2002).

The receptivity process becomes strongly nonlinear for roughness elements located in a medium range (ii). Moreover, a distinct mean flow distortion downstream of the roughness element results in a modified stability behaviour of the boundary layer. For two-dimensional roughness elements the evolving flow structures are, at first, two-dimensional before three-dimensional structures arise further downstream in the process of transition (Tani 1961; Klebanoff & Tidstrom 1972). In contrast, a three-dimensional roughness element in the medium height range (ii) leads to the formation of vortical structures at or very close to the roughness element. For a cylindrical roughness element (as used in the present study), a horseshoe shaped vortex wraps around the front side of the roughness element and a pair of spiral filaments rises vertically in the wake of the roughness as described by Tani (1961) and Tobak & Peake (1982). These observations were complemented by hot-wire measurements (Kendall 1981; Gaster, Grosch & Jackson 1994). In the region just behind the element a velocity deficit is observed in the roughness centreline region. Further downstream the mean flow distortion decreases in the centreline region whereas high- and low-speed streaks can be observed on either side of the roughness. A streak is referred to as a region of high or low mean flow velocity in spanwise direction. The vortical structures evolving in the wake are likely to originate from these velocity streaks. Further details on the flow topology, including water tunnel visualizations around a cylindrical element, are reviewed by Délery (2001). The disturbance growth, that is induced by the roughness, is most distinct in the near wake. In the far roughness wake, the streaks and, therewith, the vortical structures will eventually decrease so that a spanwise uniform base flow is recovered. The stabilization of the mean flow in the streamwise evolution counteracts the unsteady disturbance growth. Hence, in the medium roughness height range the disturbances, which result from the boundary layer roughness interaction can decay without causing transition (Ergin & White 2006).

The stability of streaks, which are excited by a mean flow distortion (as for example a roughness element) in a laminar boundary layer, has been studied numerically (Wu & Luo 2003). For a small-amplitude distortion, it is seen that the instability modes can be treated as modified TS waves with increased growth rates compared with linear theory. Moreover, the instability modes are confined to the region of the mean flow distortion. For large-amplitude distortions, however, the flow becomes inviscidly unstable, resulting in instability modes at frequencies, which are considerably higher compared to those of the TS wave instability. The investigations by Andersson *et al.* (2001) indicate a critical streak amplitude of about one quarter of the free-stream velocity for the onset of secondary instabilities. Cossu & Brandt (2002, 2004) focused on the boundary layer stability behaviour in the presence of spanwise periodic streaks with respect to spanwise invariant viscous instability waves. They could show a stabilizing effect with increasing streak amplitude, since the spanwise modulation

https://doi.org/10.1017/jfm.2014.499 Published online by Cambridge University Press

of the initially two-dimensional TS waves can decrease the growth rates of the viscous instability. These findings have been experimentally confirmed in the work of Fransson *et al.* (2004, 2005). They used a roughness array, which was located upstream of the critical Reynolds number for TS wave growth, to generate a spanwise modulated base flow, in which the TS waves have been induced further downstream. A stabilizing effect on the TS instability due to a roughness modulated mean flow was also observed in the numerical work of Piot, Casalis & Rist (2008).

For roughness heights close to or larger than the boundary layer displacement thickness (iii), a strong mean flow distortion causes highly nonlinear effects. Hence, transition occurs very close to the roughness element and is often referred to as bypass transition. Critical roughness Reynolds numbers for cylindrical elements are found of the order of $R_{h,crit} = 440$ (Gregory & Walker 1956) and $R_{h,crit} = 500$–800 (Tani 1961). However, it was found that the value for $R_{h,crit}$ is subject to the roughness height-to-diameter ratio, the pressure gradient and the turbulence intensity. Moreover, the critical Reynolds number exhibits a strong dependency on the roughness location with regard to the leading edge, that is $R_{h,crit}$ decreases with increasing Re_{δ_1}, due to the altering stability characteristics of the boundary layer in the streamwise evolution (see e.g. Tani (1961); $R_{\delta_1} = u_\delta \delta_1 / \nu$ with u_δ being the velocity at the boundary layer edge and δ_1 the displacement thickness). First detailed investigations of a high roughness element (mainly a hemisphere was used) interacting with a laminar boundary layer were conducted by Acarlar & Smith (1987) and Klebanoff, Cleveland & Tidstrom (1992). Different mechanisms appeared to lead to turbulence in the inner (close to the surface) and outer region hinted at by two inflection points in the mean flow velocity profile. Vortices close to the surface were seen to provide a strong mixing of high- and low-speed regions leading to turbulent flow, which also propagates into the outer region. There, hairpin vortices were observed for roughness heights above a critical value, whose origin and role in influencing transition, however, remained unclear. DNS simulations by Matheis, Huebsch & Rothmayer (2004) showed good agreement with the experiments by Acarlar & Smith (1987) concerning the flow topology. Recent experiments (Ergin & White 2006) aimed at linking the steady and the unsteady disturbances evolving in the roughness wake. The mean flow inflection points in wall-normal and spanwise direction were seen to coincide with the maximum unsteady disturbance growth. The authors attribute this observation to a Kelvin–Helmholtz-type instability mechanism that may be responsible for the disturbance growth in the wake of supercritical roughness elements.

Today, roughness-induced transition is of particular interest for the design of highly efficient wind turbine blades, since the blade leading edge region can easily be contaminated by dust, salt or surface erosion. Wind turbines operate in the lower mixing layer of the atmosphere, ranging from the near-surface Prandtl layer up to the lower part of the Ekman layer (Foken 2006). In these layers, vortical disturbances are present, which can be described by the Kolmogorov energy spectrum. The interaction of the blade boundary layer, including the roughness element, with these vortical inflow disturbances can, in principle, be described, as a receptivity process. However, the number of free parameters is very high, since receptivity due to free-stream disturbances depends on the frequency and orientation of the vorticity vector, the local curvature of the airfoil and the near-wake field of the roughness (Saric *et al.* 2002; Herr 2004). In the present case, it is therefore assumed that the outer disturbances already entered the boundary layer upstream of the roughness, that is close to the leading edge, which exhibits high receptivity due to strong changes in surface curvature. Downstream, these disturbances are reduced to a set of modes due

https://doi.org/10.1017/jfm.2014.499 Published online by Cambridge University Press

to the selective filtering of the boundary layer. The remaining modes can be regarded as TS waves in a limited streamwise and spanwise wavenumber range. Therefore, the interaction of a perturbed laminar boundary layer with a roughness element is of particular interest and shortly reviewed in the following.

Crouch (1997) studied the local receptivity to secondary instabilities for a TS wave scattering at a protruding roughness element. For low TS wave amplitudes, subharmonic modes are likely to be dominant within secondary instability, whereas for higher TS wave amplitudes the fundamental mode prevails. Findings from a plane channel flow investigation (Ustinov 1995) suggest that the scattering of a two-dimensional TS wave at a three-dimensional bump results in an excitation of oblique modes at the fundamental mode frequency. The growth of the oblique modes leads to secondary instability modes, which grow in a wedge-shaped region downstream of the roughness. It is seen that the wedge opening angle increases with the primary TS wave amplitude. More recent theoretical investigations (Wu & Hogg 2006), which are based on the triple-deck theory, indicate that the TS wave scattering at a small height roughness element in a laminar boundary layer might slightly decrease the TS wave amplitude downstream of the roughness.

For roughness elements in the medium height range a highly oblique wave train as a result of an initially two-dimensional TS wave scattering at a three-dimensional roughness was also observed in boundary layer flows (Rist & Jäger 2004; Piot *et al.* 2008). Piot *et al.* (2008) found that the interaction of the TS wave with the roughness, which they refer to as local receptivity towards secondary instabilities, ends rapidly downstream of the roughness, whereas the mean flow is still distorted by the roughness interaction. Disregarding the near roughness wake, the streamwise evolution of streaky eigenmodes (secondary instability modes) computed with a DNS were observed to be in good agreement with a bi-global stability approach. Bakchinov *et al.* (1995) investigated the disturbance evolution for a periodically modulated spanwise flow. For low spanwise modulation the disturbance frequencies were typical for TS wave instability, but the growth was more distinct compared with linear theory. For stronger spanwise modulated base flows higher-frequency disturbances occurred, which propagated with an increased phase velocity. This instability seemed of local, inviscid nature and was associated with the spanwise inflection points similarly as described more recently by Ergin & White (2006).

For roughness heights in a medium range and small TS wave amplitudes, experimental investigations (de Paula, Würz & Medeiros 2008) show a decay of three-dimensional structures generated by the roughness as the waves propagate downstream. In contrast, for high amplitudes of the incoming two-dimensional TS wave a growth of spanwise modes can be observed and results in the formation of an oblique wave train downstream of the roughness element. Dominant spanwise wavenumbers are observed for modes with propagation angles near $\Theta = 45°$ (with $\Theta = \mathrm{atan}(\lambda_s/\lambda_z)$ and λ_s and λ_z being the streamwise and spanwise wavelength, respectively). Moreover, investigations by Wang (2004) show the most pronounced interaction in-between the roughness element and the convective boundary layer instability for modes near the upper branch of the neutral instability curve at the roughness position.

Recently, experimental investigations by de Paula *et al.* (2013) have highlighted the role of low-frequency disturbances in the transition development initiated by modulated TS waves. This scenario seems closely related to the present experiments (compare § 3), for which an oblique wave train evolves downstream of a medium roughness height element. In this context, a brief overview is given on the growth of

https://doi.org/10.1017/jfm.2014.499 Published online by Cambridge University Press

low-frequency disturbances in the nonlinear stages of boundary layer transition. Breuer, Cohen & Haritonidis (1997) observed low-frequency, high-spanwise-wavenumber modes in a second stage of the transition process, that succeeded a stage with dominant subharmonic growth. Accordingly, the low-frequency disturbances were understood as subsequent nonlinear mode interactions. A further explanation for the growth of low-frequency modes is given by the concept of phase-locked wave interactions, which was introduced for the Rayleigh instability (Wu & Stuart 1996) and more recently applied to a flat-plate laminar boundary layer (Wu, Stuart & Cowley 2007). Based on a high-Reynolds-number asymptotic theory, an interaction of a planar and an oblique TS mode is considered, which share approximately the same phase speed and result in the generation of modes at the sum and the difference frequency. In the following, the difference mode experiences super-exponential growth, whereas the sum mode is considerably less pronounced and restricted to the critical layer. In a first nonlinear stage, only the growth behaviour of the difference mode is affected, whereas the modal shape can still be described with linear theory. In a second stage, the eigenfunction is deformed, whereas the planar TS mode still evolves according to linear theory. A fully interactive stage is reached when self-interactions in between the difference modes and a back effect on the planar mode are present. Compared with subharmonic resonance (compare e.g. Corke & Mangano 1989; Kachanov 1994), this phase-locked wave interaction mechanism works under less restrictive conditions. Therefore, Wu *et al.* (2007) suggest that the above-described mechanism might be responsible for a growth of low-frequency, broadband disturbances in the nonlinear stages of transition. In recent experimental investigations by de Paula *et al.* (2013), a distinct growth of self-generated difference modes was observed, when two fundamental waves were excited in an APG laminar boundary. It is seen that the difference mode is amplified by a linear instability at first. An order-of-magnitude analysis for the onset of the first nonlinear stage described by Wu *et al.* (2007) is in agreement with the experimental findings. Moreover, the nonlinear interactions in the experiments occur in the critical layer for modes with approximately equal phase speeds in agreement with the phase-locked interaction mechanism described by Wu *et al.* (2007). Hence, the most dominant mechanism for the growth of the low-frequency difference modes in the first, weakly nonlinear stage is associated with a 'subharmonic-type frequency-detuned resonance' between the difference and the fundamental modes (de Paula *et al.* 2013).

The subject of the present paper is to investigate the evolution of fundamental TS modes in the wake of medium-height roughness elements. Upstream of the roughness the TS wave growth is most distinct for two-dimensional modes, whereas the interaction with the roughness results in an excitation of highly oblique fundamental modes. A focus is set on the evolution of low-frequency combination modes, which can result from the interaction of planar and oblique fundamental modes (see the discussion above). At first, the development of uncontrolled (that is natural, broadband) disturbances downstream of the roughness is investigated. Therewith, an overview on the different stages of transition is obtained when a natural, non-restrictive mode selection is possible. In a second step, controlled disturbances are excited upstream of the roughness and tracked downstream with temporally phase-locked measurements to quantify the disturbance evolution in the roughness wake in detail. Moreover, the introduction of controlled disturbance modes gives an indication on the effect that a higher inflow turbulence level would have. As discussed above, this is especially relevant in the context of wind turbine applications. In the experiments a cylindrical-shaped roughness element is placed in an airfoil leading edge region

https://doi.org/10.1017/jfm.2014.499 Published online by Cambridge University Press

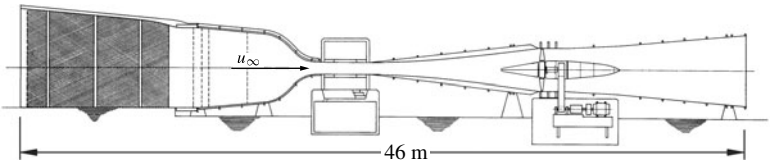


FIGURE 1. Side view of the LWT of the IAG.

and the chord-based Reynolds number is $Re = 6\,000\,000$ to achieve a close alignment with operational conditions of wind turbines.

The paper is organized as follows: the experimental set-up and methods of data analysis are described in § 2. The experimental results are discussed in § 3 and the main findings are summarized in § 4.

2. Experimental set-up and data analysis

2.1. *Wind tunnel*

The experiments were carried out in the Laminar Wind Tunnel (LWT) of the Institute of Aerodynamics and Gas Dynamics (IAG) in Stuttgart (Wortmann & Althaus 1964). The LWT is an open-return wind tunnel of Eiffel type (figure 1). An effective contraction ratio of 20:1 and several screens in the inlet section of the LWT lead to a very low (unseparated) longitudinal turbulence level of $Tu_x = 2 \times 10^{-4}$ obtained in a frequency range of $f = 10$–5000 Hz for a free-stream velocity of $u_\infty = 30$ m s^{-1} (Herr 2004). The transverse turbulence intensities are in the same order of magnitude. Up to 98 % of the longitudinal turbulence intensity is contained within a frequency range from $f = 10$–150 Hz. For higher frequencies, velocity fluctuations monotonically roll-off and are below the electronic noise of standard hot-wire measurement technique. The closed test section has a cross-section of 0.73 m $\times$ 2.73 m and a length of 3.15 m. The airfoil models are mounted vertically with a spanwise length of 0.73 m. Gaps between the model and the wind tunnel walls are carefully sealed. The test section is surrounded by a low-pressure chamber in order to avoid flow passing into the test section through leakages. The diffusor section of the LWT is equipped with noise absorbing foam, significantly reducing the background noise propagating upstream from the fan into the test section (Plogmann & Würz 2013). The wind tunnel sucks air directly from the atmosphere, leading to small changes of the inflow parameters with time. During the measurements the free-stream velocity and not the Reynolds number was kept constant due to the quadratic dependency of the non-dimensional frequency parameter ($F = 2\pi f \nu / u_\delta^2$) on the free-stream velocity. The calculation of the stagnation pressure is, therefore, based on continuously measured ambient conditions (total pressure, total temperature and humidity).

2.2. *Airfoil design and model*

Experimental investigations in an airfoil leading edge region at high Reynolds number are usually complicated due to a thin boundary layer and a high surface curvature. In the present experiments the wind tunnel model was, therefore, geometrically upscaled resulting in a high Reynolds number ($Re = 6\,000\,000$) at low free-stream velocity ($u_\infty = 20$ m s^{-1}). In the leading edge region the pressure distribution of the newly developed BE72 airfoil section is closely related to the NACA 64_3-418, which can

https://doi.org/10.1017/jfm.2014.499 Published online by Cambridge University Press

be regarded a typical airfoil for wind turbine applications. In the trailing edge region the pressure rise of the BE72 was designed more progressive to shorten the model to a realized chord length of $c = 2.4$ m. However, since the pressure distribution in the leading edge region was not changed the results can still be attributed to a full-size Reynolds number of $Re = 6\,000\,000$ although the chord-based Reynolds number of the BE72 airfoil section is only $Re = 3\,000\,000$. For further details on the model design compare with Plogmann, Würz & Krämer (2012*a*).

The BE72 model consists of two parts. The leading edge section ($x/c = 0$–0.4) was built from reinforced fibreglass using numerically controlled milled molds. In the measurement region ($0.1 < x/c < 0.4$) a highly polished brass sheet, which was carefully bent to the model contour, is inserted. In addition, the measurement region is equipped with 63 pressure orifices allowing for the measurement of the static pressure distribution. The rear part of the model ($x/c = 0.4$–1) was built in positive technique. After wet-sanding and polishing, the remaining RMS (root mean square) surface roughness height in the leading edge section is of the order of $R_z = 0.5$ μm (measured with a Diavite DH-5 precision surface measuring system).

The single roughness element is of cylindrical shape and has a diameter of $d_r = 20$ mm. It is integrated into the model at a streamwise location of $x/c = 0.15$. The roughness surface is thoroughly adjusted to the curved model contour. Employing a linear actuator the roughness element can be displaced in a range from $h/\delta_{1,ref} = 0$–2. Closed-loop positioning with a minimal incremental motion <0.1 μm leads to a very high accuracy in the adjustment of the roughness height. Moreover, the actual roughness height is measured with a laser-triangulation system with a resolution of 0.15 μm corresponding to 0.2 % of the boundary layer displacement thickness at the position of the roughness element ($\delta_{1,ref}$).

For the controlled excitation of boundary layer disturbance modes (TS waves), a specially designed disturbance source is used (compare e.g. Würz *et al.* 2012). A very thin slit (length = 320 mm, width = 0.2 mm) is integrated surface flush into the model at a streamwise position of $x/c = 0.1$ and via tubes (length = 2 m, spanwise spacing $dz = 2.5$ mm) connected to 128 individually controllable micro-loudspeakers (Sennheiser CX300). The loudspeakers are installed in an airtight box and balanced by a static pressure port at the streamwise slit position. A 128-channel digital signal generator with a memory of 8192 points per channel provides the signal for the loudspeakers (de Paula *et al.* 2010, 2013). A common quartz-based clock is used to trigger all 128 channels and provides the sample clock for the data acquisition in order to assure strictly phase-locked measurements (compare § 2.3). Employing this set-up, TS waves in a wide streamwise and spanwise wavenumber range can be excited with a high linearity in amplitude and sufficiently small scattering in phase (compare § 3.1). Upstream of the source the disturbance amplitude decays rapidly, that is the amplitude 20 mm upstream of the disturbance source is only 4 % of the amplitude measured 20 mm downstream for a frequency of $f = 549$ Hz (compare figure 3). This is in good agreement with previous theoretical (Terentev 1981) and experimental (Würz *et al.* 2012) findings.

2.3. *Data acquisition and analysis*

The main measurements have been performed using a constant-temperature hot-wire anemometer. A boundary layer probe of type 55P15 with a 5 μm gold-plated tungsten wire was used. The hot-wire calibration is based on the King's law with the coefficients optimized for a minimum standard deviation. During measurements a

https://doi.org/10.1017/jfm.2014.499 Published online by Cambridge University Press

static pressure probe determines the velocity at the boundary layer edge (u_δ), which is used for a linear *in situ* correction of the hot-wire reading. Both, the hot-wire and the static pressure probe, are mounted to a traversing system allowing for computer controlled boundary layer scans in wall-normal and spanwise direction, respectively. The traversing accuracy is 5 μm in wall-normal direction and 100 μm in spanwise direction.

The hot-wire probe was operated with a DISA 55M10 bridge using an overheat ratio of 1.8. The hot-wire signal was split into AC and DC part. For the low-pass filtering an active low pass with a cut-off frequency of $f_{cl} = 1$ Hz was used. The AC part was high-pass filtered with a passive RC filter ($f_{ch} = 50$ Hz). Due to a high sampling rate ($f_s = 15\,625$ Hz, approximately 20 times the relevant signal frequency) and a strong decay of the spectral density in the high-frequency range, no additional anti-aliasing filter was necessary. However, the analogue-to-digital (AD) converter is equipped with a $f_{cl} = 40$ kHz low-pass filter, which minimizes the effect of very high-frequency noise. AC and DC signals are acquired with an 18-bit AD converter (NI-USB 6289). In the case of controlled disturbance input the data acquisition is strictly phase-locked to the signal generation (compare § 2.2)

For each measurement point a total of 32 768 samples was recorded. In the post-processing the AC part is corrected for the transfer function of the high-pass filter. AC and DC parts are, then, summed up in order to calculate velocities from the voltage signal. Prior to a fast Fourier transformation (FFT) the fluctuation velocities are split into 8 blocks of 4096 samples and ensemble averaged in the temporal domain provided that controlled disturbances are excited upstream of the roughness element. Therewith, the signal-to-noise ratio is increased by a factor of $\sqrt{8}$. However, if no phase-locked disturbances are excited upstream of the roughness, the velocity spectra are ensemble averaged in the spectral domain. For the FFT a rectangular window without overlap was applied, since (i) the obtained time record is sufficiently long. Moreover, in case of excited boundary layer disturbances (ii), the introduced modes exactly correspond to single Fourier series coefficients. Spanwise boundary layer measurements were interpolated to an equidistant grid with a constant spanwise domain of $-7.5 \leqslant z/d_r \leqslant 7.5$. Spanwise wavenumber spectra were, then, obtained by decomposing the interpolated measurements via complex FFT. Finally, the spanwise wavenumber $\beta = 2\pi/\lambda_z$ is normalized with the roughness diameter d_r. Hence, $\beta d_r = 2\pi$ corresponds to a wavelength equal to the roughness diameter.

3. Results and discussion

3.1. *Base flow characteristics*

A PSI pressure scanning system (ESP 64 HD) is used to obtain the pressure distribution with the boundary layer traverse placed inside the test section at $x/c = 0.4$ (figure 2*a*). Streamwise relocation of the traversing system showed the upstream influence to be small (Plogmann *et al.* 2012*a*). A comparison with calculated (XFOIL Drela 1989) pressure distributions shows a small offset to lower c_p values in the experiments due to an increased local velocity, which is caused by blockage effects resulting from the large model size. Therefore, the measured pressure distribution is used for the calculation of the boundary layer profiles based on a finite-difference scheme proposed by Cebeci & Smith (1974). That is, the pressure distribution is fitted with fourth-order piecewise continuous polynomials in a least-squares sense, before the boundary layer profiles are calculated starting from the stagnation point.

https://doi.org/10.1017/jfm.2014.499 Published online by Cambridge University Press

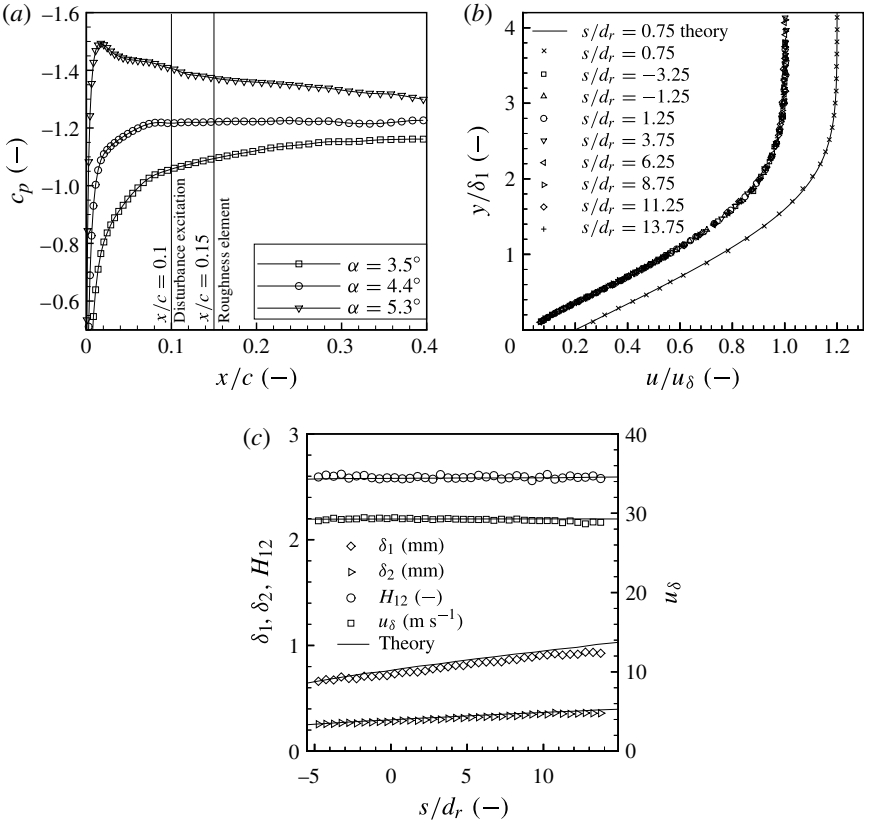


FIGURE 2. Base flow characteristics: (*a*) pressure distribution, (*b*) boundary layer mean flow velocity profiles, shifted by $u/u_\delta = 0.2$ at $s/d_r = 0.75$ and (*c*) integral boundary layer parameters (*b*,*c* for $\alpha = 4.4°$).

The linear stability characteristics are, then, calculated locally based on a shooting method according to Conte (1966).

For the measurements three characteristic pressure distributions are selected in the vicinity of the upper edge of the low-drag bucket of the airfoil polar, hence, close to best glide ratio. In particular, the boundary layers have a favourable (FPG), close to zero (ZPG) and an adverse pressure gradient (APG) for $x/c < 0.4$ (figure 2*a*). In all cases the boundary layer is laminar up to the end of the measurement domain ($x/c < 0.3$). Boundary layer mean flow characteristics are exemplary shown for an angle of attack of $\alpha = 4.4°$ since the boundary layer roughness interaction was mainly investigated at ZPG. In that case, the velocity at the boundary layer edge (u_δ) is nearly constant within the measurement region resulting in a shape factor close to the value for a Blasius boundary layer ($H_{12} = 2.591$). Moreover, comparing the mean flow velocity profiles within the measurement region confirms a good self-similarity of the boundary layer (figure 2*b*). Here, s is referred to as the streamwise coordinate with the origin at the centre of the roughness element and the disturbance source is located at $s/d_r = -6.25$. The streamwise evolution of the integral boundary layer parameters, that is displacement thickness δ_1, momentum thickness δ_2 and shape factor H_{12} is shown in figure 2(*c*) in comparison with the values obtained by the finite difference scheme. In general, the measured and the theoretical evolution agree well. However,

https://doi.org/10.1017/jfm.2014.499 Published online by Cambridge University Press

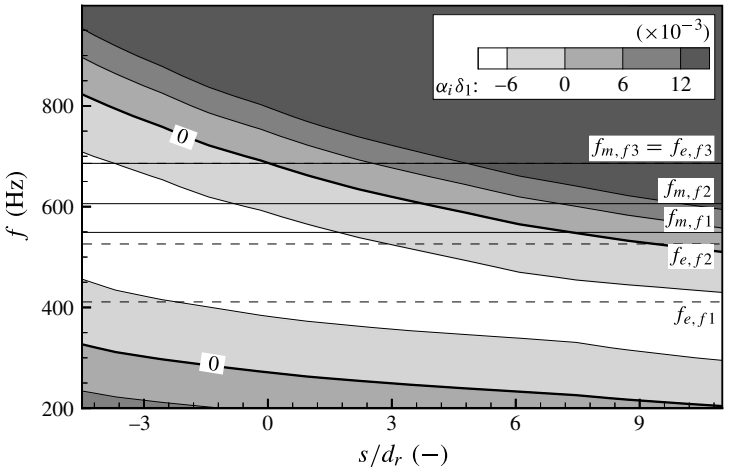


FIGURE 3. Linear stability diagram for two-dimensional TS waves in ZPG boundary layer, excited fundamental TS wave frequencies indicated with solid (f_m case) and dashed (f_e case) lines, ($f_{m,f3} = f_{e,f3}$).

Pressure gradient	$dc_p/d(x/c)$ (—)	β_H (—)	$H_{12,ref}$ (—)	$\delta_{1,ref}$ (mm)	$\delta_{2,ref}$ (mm)
Favourable	−0.62	0.041	2.54	0.67	0.264
Zero	≈0	0	2.59	0.72	0.278
Adverse	0.46	−0.031	2.64	0.78	0.295

TABLE 1. Integral boundary layer parameters at the roughness position depending on the pressure gradient.

the gradients for the measured distributions of the boundary layer displacement and momentum thickness are slightly lower in comparison with the theoretical values. Table 1 summarizes the integral boundary layer parameters at the roughness position depending on the pressure gradient. The Hartree parameter β_H is obtained based on the assumption of a self-similar boundary layer in compliance with the observations in figure 4(*b*,*c*). In the following, both the height of the roughness element h and the wall-normal coordinate y are normalized with the displacement thickness at the roughness position $\delta_{1,ref}$, whereas the streamwise s and the spanwise z coordinate are normalized with the roughness diameter d_r with the spanwise roughness centre at $z/d_r = 0$. Mean flow velocities are related to the local boundary layer edge velocity u_δ.

At the roughness position, two-dimensional TS waves are amplified in a frequency range $270 < f < 690$ Hz as can be inferred from the linear stability diagram (figure 3). In order to verify the agreement of the disturbance growth in the reference case (zero roughness height) with linear theory, six two-dimensional TS waves were simultaneously excited (figure 4). The maximum (wall-normal) RMS amplitude A of each eigenfunction is normalized by its initial amplitude A_0 and the phase ϕ is set to zero at the initial position ($s/d_r = -4.25$) for all TS wave frequencies. In the streamwise evolution a good agreement to linear theory (dashed line) is observed in the entire investigated frequency range for amplitude and phase. Moreover, experimental and theoretical TS wave eigenfunctions for amplitude and phase match very well as can be seen in figure 4(*c*) for a TS wave frequency of $f = 549$ Hz.

https://doi.org/10.1017/jfm.2014.499 Published online by Cambridge University Press

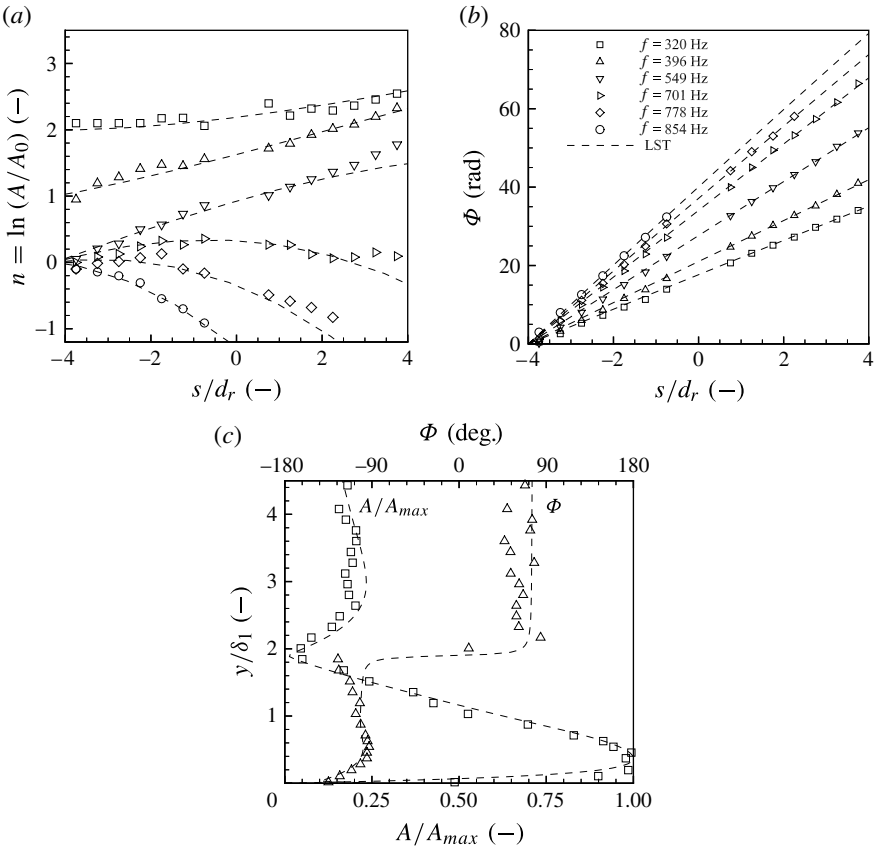


FIGURE 4. Streamwise n-factor (a) and phase (b) evolution of simultaneously excited two-dimensional TS waves and TS eigenfunction for $f = 549$ Hz at $s/d_r = 0.75$ in comparison with linear theory (dashed line) (c) for ZPG boundary layer, same legend for (a,b).

Measurements concerning the two-dimensionality of the disturbance modes at $s/d_r = 0.75$ revealed a standard deviation for the TS wave amplitude of 8 % of the mean amplitude. The corresponding standard deviation of the measured TS wave phase is 6.8°, i.d. 1.9 % of 360°, compare also Plogmann, Würz & Krämer (2012*b*).

3.2. *Boundary layer roughness interaction without controlled disturbance excitation*

At first, measurements were performed without artificial disturbance excitation meaning that all disturbances start to grow based on the uncontrolled, broadband background noise level of the wind tunnel flow. Therewith, it is seen which disturbance modes preferably interact with the roughness element. Since the background noise level of the LWT is very low (compare § 2.1) and the disturbance growth downstream of the roughness is expected to be more distinctive with increasing pressure gradient, measurements are first conducted in the APG boundary layer. The steady and unsteady disturbance evolution downstream of the cylindrical roughness element at low, medium and high roughness heights can be deduced from the shape factor H_{12} (figure 5*a*) and the streamwise velocity fluctuations u' for $f = 10$–5000 Hz (figure 5*b*), respectively. For the low height roughness element ($h/\delta_{1,ref} = 0.1$), both the

https://doi.org/10.1017/jfm.2014.499 Published online by Cambridge University Press

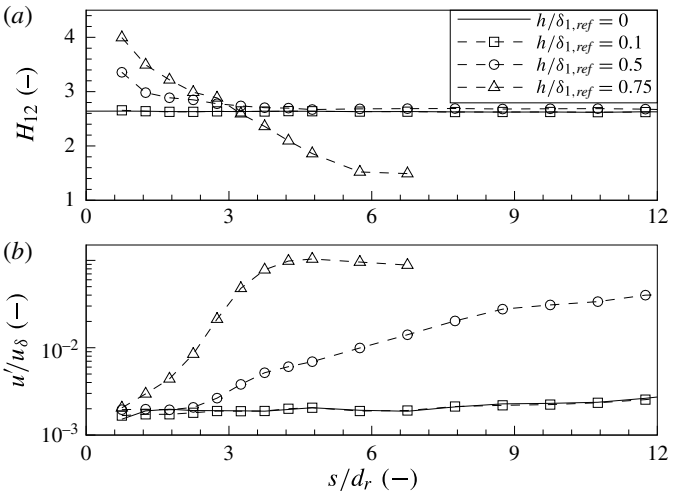


FIGURE 5. Streamwise evolution of shape factor H_{12} (a) and of streamwise velocity fluctuations u' (wall-normal maximum) (b) on roughness centreline ($z/d_r = 0$) for APG boundary layer.

steady and the unsteady flow characteristics are nearly unaffected, as can be seen from the comparison with the reference case ($h/\delta_{1,ref} = 0$). Moreover, no distinct variations in the spanwise mean flow distribution (not shown) are obvious in comparison with $h/\delta_{1,ref} = 0$ for $s/d_r > 1$. In contrast, in the medium height range ($h/\delta_{1,ref} = 0.5$ corresponding to $R_h = 196$) the shape factor is, at first, considerably increased due to a velocity deficit in the near roughness wake. Further downstream the shape factor approaches the value of the undisturbed laminar boundary layer as the mean flow recovers from the roughness influence. The interaction with the roughness element results in an excitation of streamwise velocity fluctuations, which are continuously growing (figure 5*b*). For high roughness elements ($h/\delta_{1,ref} = 0.75$), the growth of the unsteady disturbances is increased decisively. Therefore, transition can be observed in the closer vicinity of the roughness element ($s/d_r < 5$) resulting in an almost constant disturbance level of $u'/u_\delta \approx 0.1$ in the turbulent boundary layer. Hence, the high roughness element with $R_h = 445$ is supercritical, which is in agreement with critical values of Gregory & Walker (1956) ($Re_{h,crit} = 440$) and Klebanoff *et al.* (1992) ($Re_{h,crit} = 450$) for a cylindrical roughness with $h/d_r = 1$. It is slightly lower compared with the values reported by Tani (1961) ($Re_{h,crit} = 500$–800) for cylindrical elements. However, Tani (1961) used a different criterion for the transition location, that is an intermittency factor of $\gamma = 0.5$, whereas Klebanoff *et al.* (1992) used the position when first turbulent bursts occurred. More recently, Fransson *et al.* (2005) give a value of $Re_{h,crit} = 422$ for a cylinder with $h/d_r \approx 0.3$ based on an intermittency factor of $\gamma = 0.5$ showing that the critical roughness Reynolds number decreases with the height-to-diameter ratio. The present experiment is different in terms of pressure gradient, distance from the leading edge and roughness height-to-diameter ratio, which is very low for the supercritical case ($h/d_r = 0.029$ for $h/\delta_{1,ref} = 0.75$). Moreover, the disturbance level at the roughness position, which is very low in the present case, also influences the critical roughness Reynolds number. Hence, the present value for $Re_{h,crit}$ can only be used as an approximate value with regard to the previous findings.

https://doi.org/10.1017/jfm.2014.499 Published online by Cambridge University Press

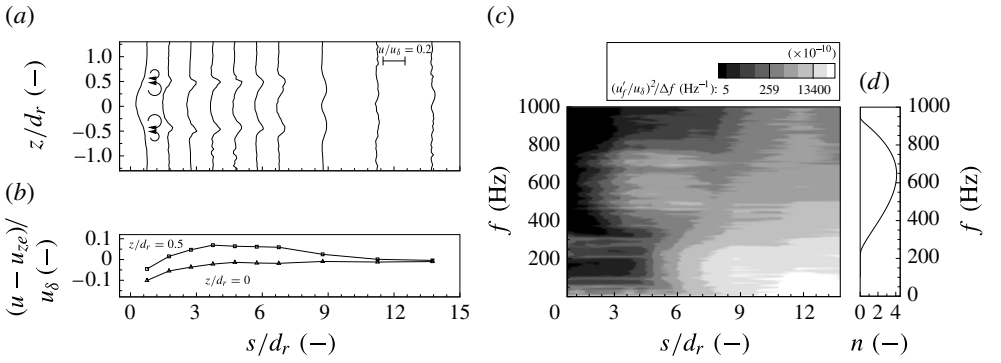


FIGURE 6. Mean flow evolution in the streamwise–spanwise plane (*a*) and streak amplitude (*b*) at $y/\delta_{1,ref} = 1.0$ and disturbance evolution on roughness centreline (*c*) for $h/\delta_{1,ref} = 0.5$ and APG boundary layer, *n*-factor at $s/d_r = 0$ based on linear theory (*d*).

In the following, further light is shed on the flow topology downstream of the medium-sized roughness elements, that is $h/\delta_{1,ref} = 0.2$–0.5. In the near wake the highest mean flow distortion is present in the centreline region (figure 6*a*). Further downstream the mean flow distortion in the centreline region decreases, whereas high-speed streaks form at spanwise positions $z/d_r = \pm 0.5$ corresponding to the edges of the roughness element (figure 6*b*). Here, u_{ze} is the mean flow velocity at the undisturbed spanwise edge of the measurement domain. Moreover, weakly distinct low-speed streaks are present at the outer edges of the high-speed streaks (compare also Plogmann, Würz & Krämer 2014). The formation of these high- and low-speed streaks hints at the presence of two counter-rotating vortex pairs as indicated in figure 6(*a*). In the centreline region low-momentum fluid is shifted off the wall (lift-up effect described by Landahl 1980) by the inner (trailing) vortex pair, whereas both vortex pairs entrain high momentum fluid towards the wall at $z/d_r = \pm 0.5$. Finally, the outer (weakly distinct) low-speed streaks are associated with the outer (horse shoe) vortex pair. In the streamwise evolution, these streaks and, therewith, the vortices persist at a constant spanwise position in agreement with previous experimental findings in the wake of a cylindrical roughness element (Wang 2004). The high-speed streaks are most pronounced for $s/d_r = 2$–5 with an amplitude of up to 8 % of the velocity at the boundary layer edge, whereas farther downstream, the relaxation of the mean flow towards a spanwise uniform flow implies a significant damping of the streaks caused by the roughness element (figure 6*a*,*b*).

The flow topology downstream of the medium-sized roughness element is seen to be in agreement with previous findings in the literature (compare e.g. Délery 2001; Piot *et al.* 2008). Hence, the observed tails of a horse-shoe vortex in the roughness wake imply that in the medium roughness height range a horse-shoe vortex is wrapped around the front side of the roughness, so that a small separated region forms upstream of the roughness. In the present experiments this region is restricted to the near-wall region ($y/\delta_{1,ref} < 0.2$) and can, therefore, not be investigated with the hot-wire measurement technique. Additional information on the mean flow field downstream of the medium height roughness element can also be found in Plogmann *et al.* (2014).

In the following, the spectral disturbance evolution for $h/\delta_{1,ref} = 0.5$ on the roughness centreline is discussed. Figure 6(*c*) shows the wall-normal maximum of the disturbance amplitude extracted for each single frequency (Fourier coefficient)

https://doi.org/10.1017/jfm.2014.499 Published online by Cambridge University Press

and plotted as a function of the streamwise coordinate s. Immediately downstream of the roughness ($s/d_r < 4$) the disturbance growth is most distinctive for high-frequency modes $400 < f < 800$ Hz. A comparison with the n-factor distribution at $s/d_r = 0$ in the undisturbed case ($h/\delta_{1,ref} = 0$, figure 6d) shows that in this frequency range maximum disturbance amplitudes are predicted by linear theory. Hence, downstream of the roughness those disturbances, which grew maximal up to the position of the roughness, are most distinct, at first. Below $f = 300$ Hz a disturbance growth is not observed for $s/d_r < 4$. For $s/d_r > 5$ the relaxation of the mean flow towards a spanwise uniform state (compare figure 6a) is inherent with a slight decay of the high-frequency disturbance modes. In contrast downstream of $s/d_r = 4$, a rapid growth of low-frequency modes ($f < 300$ Hz) is observed, which are stable according to linear theory for $f < 200$ Hz in the undisturbed reference case (zero roughness height). Only less further downstream the disturbance spectrum is dominated by these low-frequency modes and, eventually, the disturbance spectrum takes on a turbulent character. Hence, the growth of the low-frequency modes seems to be a significant mechanism for tripping turbulence in the far wake provided that the initial disturbance level at the roughness is low (compare § 2.1). In the following measurements with a controlled disturbances excitation upstream of the roughness element are discussed to gain further phase-locked data on the disturbance evolution especially with regard to the low-frequency modes and a possible explanation for their rapid growth in the far roughness wake.

3.3. *Controlled disturbance excitation upstream of medium roughness height elements*

As the disturbance growth in the near wake of the medium height roughness element were most pronounced for $400 < f < 800$ Hz (compare the last paragraph), controlled disturbances were excited in this frequency range. At first, two-dimensional disturbance modes at fundamental frequencies $f_{f1} = 549$ Hz, $f_{f2} = 606$ Hz and $f_{f3} = 686$ Hz were simultaneously excited upstream of the roughness for $h/\delta_{1,ref} = 0.3$ in the ZPG boundary layer ($\alpha = 4.4°$). In contrast to the results mentioned in § 3.2, experiments were now performed in the ZPG boundary layer since the amplitude of the dominant disturbances is no longer prescribed by the natural, uncontrolled background noise level, but can be adjusted in a controlled manner by the disturbance source for the excited modes. Moreover, the controlled disturbance evolution in the ZPG case is considered as the reference and later (§ 3.6) compared with the APG and FPG case. At the position of the roughness element the maximum (wall-normal) RMS amplitude of each mode is adjusted to $A_m/u_\infty = 0.02\,\%$ giving a total RMS amplitude of $A_m/u_\infty = 0.035\,\%$ for the three excited fundamental modes.

The mean flow distribution downstream of the roughness at $h/\delta_{1,ref} = 0.3$ is shown in figure 7. In the near wake a considerable velocity deficit is observed and the mean flow velocity profile on the roughness centreline (figure 7c) has an inflectional nature. Based on previous investigations (e.g. Délery 2001) it is known that a small separation bubble forms in the near wake of medium height elements. The comparison with the mean flow velocity profile at $s/d_r = 0.75$ (that is, $\Delta s/d_r = 0.25$ downstream of the roughness rear edge) shows that this separation is limited to the immediate wake in the present case (figure 7c). A comparison with the evolution in the unperturbed (without disturbance excitation) case at $h/\delta_{1,ref} = 0.5$ (figure 6a) shows good qualitative agreement in the formation of the high- and low-speed streaks observed in the near wake. However, the streak amplitude is less distinct with the roughness height (compare figures 6b and 7b). Good compliance is also obvious for

https://doi.org/10.1017/jfm.2014.499 Published online by Cambridge University Press

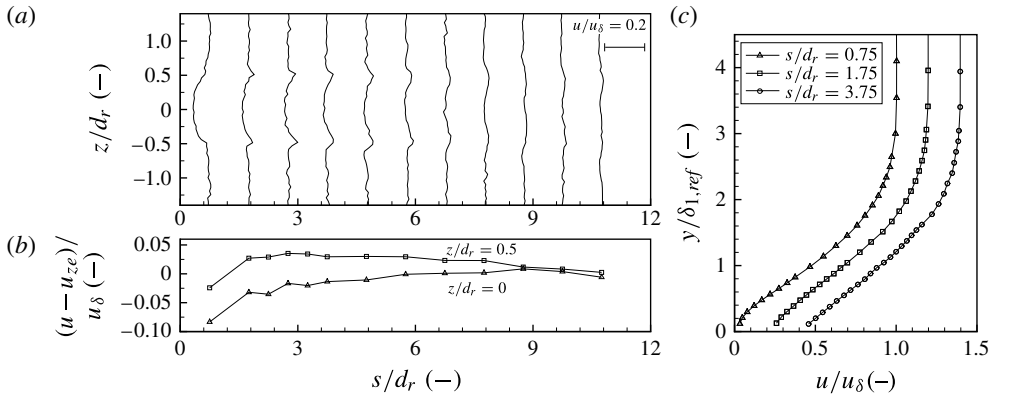


FIGURE 7. Mean flow evolution in the streamwise–spanwise plane at $y/\delta_{1,ref} = 0.9$ (*a*), streak amplitude (*b*) and mean flow profiles on roughness centreline (*c*) for $h/\delta_{1,ref} = 0.3$ with controlled disturbance excitation of fundamental modes $f_{f1} = 549$ Hz, $f_{f2} = 606$ Hz and $f_{f3} = 686$ Hz.

the mean flow relaxation towards a spanwise uniform state in the far roughness wake of the two roughness elements at $h/\delta_{1,ref} = 0.3$ and $h/\delta_{1,ref} = 0.5$. Moreover, this comparison shows, that within the measurement region the qualitative development of the mean flow structures is hardly affected by the pressure gradient (APG in figure 6 and ZPG in figure 7). If not stated otherwise, the following results relate to the ZPG boundary layer case.

3.3.1. *Evolution of fundamental modes*

Figure 8(*a*) shows the streamwise evolution of the maximum wall-normal amplitude (A_m) of the excited fundamental modes on the roughness centreline. For reference figure 8(*a*) includes a boundary layer spectrum at $s/d_r = 0.75$ for the zero-roughness height case with (red) and without (black) disturbance excitation showing that the three excited fundamental modes are well above the noise level. In the near wake of the roughness ($s/d_r < 4$), the growth of the fundamental modes is substantially increased for $h/\delta_{1,ref} = 0.3$ in comparison with the disturbance evolution without roughness element. In contrast to the reference case the growth is, at first, most pronounced for the mode with the highest frequency ($f_{f3} = 686$ Hz), which is damped for $h/\delta_{1,ref} = 0$ downstream of the roughness position. For $s/d_r > 3$ the disturbance growth in the roughness wake levels off resulting in a local disturbance maximum at $s/d_r \approx 4$, which appears rather independent of the disturbance mode frequency for the excited modes f_{f1-3}. A comparison with the evolution of the shape factor (figure 8*a*, top) reveals that the disturbance growth becomes less pronounced with the stabilization of the mean flow (compare also figure 7*c*) and that the peak in the disturbance evolution coincides roughly with the position, at which the initial shape factor ($H_{12} = 2.59$) of the boundary layer is recovered. Further downstream ($s/d_r > 7$), the growth/decay of the fundamental modes is similar compared with the reference case, showing that the undisturbed ($h/\delta_{1,ref} = 0$) boundary layer stability characteristics of the fundamental modes are recovered in the far wake. However, the interaction of the roughness element results in an increased disturbance amplitude. The above described observations are in line with findings by Wang (2004) showing that a TS

https://doi.org/10.1017/jfm.2014.499 Published online by Cambridge University Press

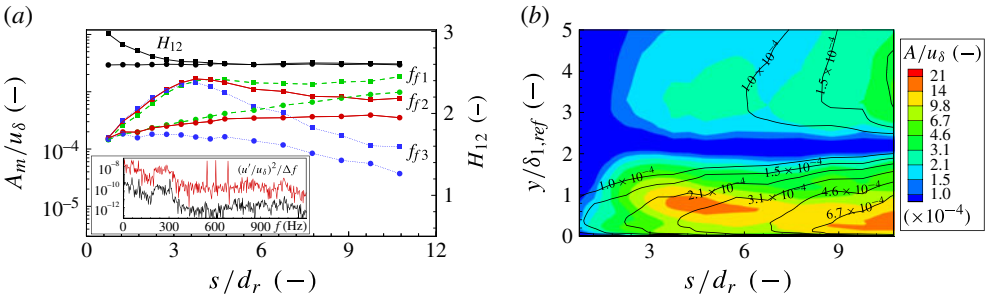


FIGURE 8. Streamwise amplitude (A_m) evolution of fundamental modes $f_{f1\text{–}3}$ and shape factor for $h/\delta_{1,ref} = 0$ (circle) and $h/\delta_{1,ref} = 0.3$ (square) including boundary layer spectra at $s/d_r = 0.75$ and $y/\delta_{1,ref} = 0.4$ for the reference case ($h/\delta_{1,ref} = 0$) without (black) and with (red, shifted by 2 decades) disturbance excitation (*a*) and evolution of $f_{f1} = 549$ Hz disturbance mode eigenfunction for $h/\delta_{1,ref} = 0.3$ (coloured contours) and for $h/\delta_{1,ref} = 0$ (black contour lines) (*b*) on roughness centreline.

wave downstream of a three-dimensional bump in the medium height range exhibits, at first, an excess growth, but can eventually recover linear stability characteristics.

Without roughness element ($h/\delta_{1,ref} = 0$), two peaks in the inner ($y/\delta_{1,ref} = 0.4$) and outer ($y/\delta_{1,ref} \approx 3$) region of the boundary layer are obvious in the disturbance mode eigenfunction (figure 8*b*, black contour lines) in compliance with linear theory for a two-dimensional mode (compare also figure 4*c*). Downstream of the medium height roughness element the strong growth of the fundamental modes for $s/d_r < 4$ is associated with the onset of a second peak in the near-wall region of the disturbance mode function (figure 8*b*, coloured contours). In contrast to the near-wall maximum of a two-dimensional mode, which is located close to $y/\delta_{1,ref} = 0.4$, the peak associated with the roughness interaction is observed at $y/\delta_{1,ref} \approx 0.9$ hinting at a growth of three-dimensional modes in the roughness wake. As the structures resulting from the disturbance roughness interaction are most distinct near $y/\delta_{1,ref} = 0.9$, it is advantageous to perform spanwise boundary layer scans at that specific wall-normal position in order to capture the dominant features of the disturbance growth. In compliance previous findings by Wang (2004) suggest a disturbance maximum near $y/\delta_{1,ref} \approx 1$ in the evolution of a fundamental mode downstream of a cylindrical roughness element. Moreover, a comparison with measurements in wall-normal–spanwise (y–z) planes, which addressed the evolution of a single TS wave mode downstream of the roughness, show that the dominant features of both the mean flow and the disturbance evolution in the near- and far roughness wake can be well captured by spanwise scans at a constant wall-normal location of $y/\delta_{1,ref} \approx 0.9$–1 (see Plogmann *et al.* 2014). However, this implies that the mean flow velocity at the measurement height is slightly decreasing in the streamwise evolution.

Figure 9 shows the disturbance evolution of the fundamental modes in the streamwise–spanwise plane at $y/\delta_{1,ref} = 0.9$. Immediately downstream of the roughness, local peaks at the edges of the roughness ($z/d_r = \pm 0.5$) are obvious (figure 9*a*), whereas the amplitude in the centreline region is slightly decreased probably due to the considerable mean flow distortion in the near wake (figure 7). Then, the disturbance growth is, however, most pronounced in the centreline region for $s/d_r < 4$ with minima developing at $z/d_r = \pm 0.5$. A comparison with the mean flow evolution

https://doi.org/10.1017/jfm.2014.499 Published online by Cambridge University Press

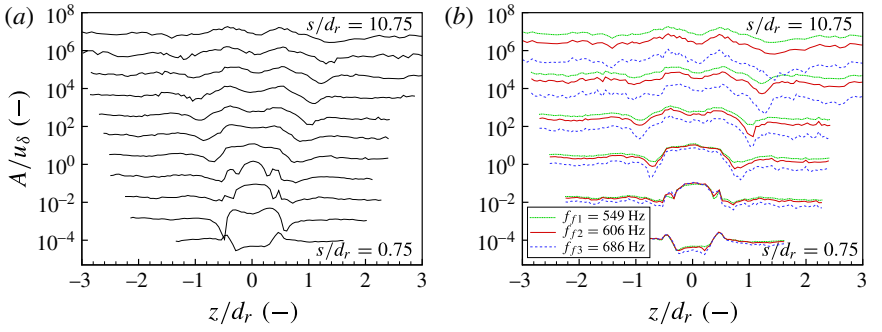


FIGURE 9. (Colour online) Evolution of fundamental mode f_{f1} (*a*) and $f_{f1\text{–}3}$ (*b*) in the streamwise–spanwise plane at $y/\delta_{1,ref} = 0.9$ for $h/\delta_{1,ref} = 0.3$, ($\Delta s/d_r = 1$ (*a*) and $\Delta s/d_r = 2$ (*b*), spanwise distributions shifted by one decade per $\Delta s/d_r = 1$).

(figure 7) shows these disturbance minima to coincide with the position of the high-speed streaks (compare also Plogmann *et al.* 2014). Hence, the high-speed streaks result in a local decrease of the disturbance mode amplitude. When the amplitude of the high-speed streaks starts to decrease ($s/d_r > 4$), the disturbance minima spread outwards (in spanwise direction) and a wavy type structure develops in between. Further downstream, the relaxation of the mean flow is accompanied by a considerable damping of the three-dimensional disturbance structures observed in the near roughness wake. Accordingly, the second near wall peak in the disturbance mode eigenfunction on the centreline is decreased and shifted towards the wall (figure 8*b*). Far downstream the disturbance mode eigenfunction reveals a similar shape in comparison to the reference case.

Figure 9(*b*) shows a comparison of the fundamental mode evolution for $f_{f1\text{–}3}$ and figure 10 the associated spanwise wavenumber spectrum for f_{f1}. The spectral amplitude in figure 10 is normalized by the two-dimensional mode amplitude at the respective streamwise position accentuating the relation between the excited two-dimensional fundamental mode and the oblique modes, which result from the disturbance roughness interaction. The spanwise structures (figure 9*b*) appear rather independent of the fundamental mode frequency (in the investigated range) suggesting that the excited spanwise modes are predominately prescribed by the roughness dimensions. In the near wake the energy of the local peaks at the edges of the roughness is spread into modes with a wide spanwise wavenumber range (figure 10). In the streamwise evolution spanwise modes are most distinct for $s/d_r < 5$ and for a spanwise wavenumber near $\beta d_r = \pm 2\pi$. Hence, the wavelength of the strongest spanwise modes is close to the roughness diameter. Moreover, the streamwise wavelength of the excited modes is in the same range, that is $\alpha_r d_r = 1.9\pi$ for $f_{f3} = 686$ Hz and $\alpha_r d_r = 2.2\pi$ for $f_{f1} = 549$ Hz. Therefore, the wave propagation angle associated with the most amplified spanwise modes is in a range $\Theta = 43\text{–}48°$ (with $\Theta = \mathrm{atan}(\lambda_s/\lambda_z)$). As the disturbance modes propagate further downstream and the mean flow resumes the undisturbed reference case ($s/d_r > 5$), a damping of the (by the roughness) generated spanwise modes is obvious in the wavenumber spectrum (figure 10). This observation is in good agreement with experimental investigations by de Paula *et al.* (2008) showing that spanwise modes excited by a cylindrical roughness decay in the streamwise evolution providing that disturbance amplitudes are rather low at the roughness position. The disturbance amplitude at the roughness

https://doi.org/10.1017/jfm.2014.499 Published online by Cambridge University Press

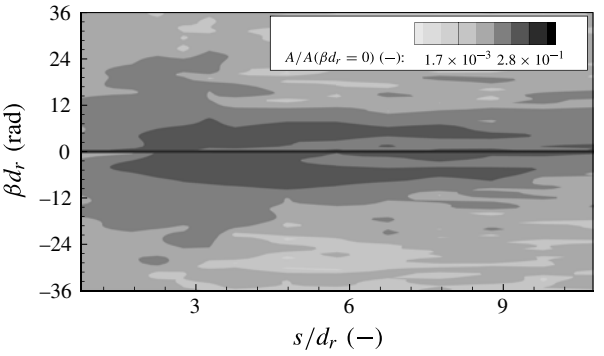


FIGURE 10. Spanwise wavenumber spectra of fundamental mode $f_{f1} = 549$ Hz for $h/\delta_{1,ref} = 0.3$ at $y/\delta_{1,ref} = 0.9$, the amplitude A is normalized by the respective streamwise amplitude of the two-dimensional mode $A(\beta d_r = 0)$.

position used in the investigations of de Paula *et al.* (2008) ($A/u_\infty = 0.45\,\%$) was even one order of magnitude higher compared with the total RMS disturbance amplitude ($A/u_\infty = 0.035\,\%$) used in the present case.

Finally, a comparison with the work by Fransson *et al.* (2005) shows agreement for the TS wave shape observed in the low-speed (centreline) region. Moreover, the second near-wall peak was observed to be significantly more pronounced in the low-speed compared with the high-speed region in line with the present investigations, in which a minimum forms in the spanwise amplitude distributions at the position of the high-speed streaks (figure 9). However, Fransson *et al.* (2005) induced the TS waves in a spanwise-modulated base flow, that is the roughness elements are located upstream of the TS wave excitation and also in the subcritical range for TS wave growth. Based on this spanwise modulated base flow the initially two-dimensional TS waves are modulated in the instance they enter the boundary layer. Hence, their growth is observed to be less distinct compared with the growth of a two-dimensional mode in a non-modulated boundary layer. In contrast, in the present experiment the roughness is located downstream of the TS wave excitation and the Reynolds number based on displacement thickness at the roughness position is considerably higher ($Re_{\delta_1,ref} = 1350$), that is the roughness is positioned far downstream of the neutral point for TS wave growth. Hence, the TS waves are exposed to the immediate wake of the roughness, in which the boundary layer is destabilized leading to a substantially increased TS wave growth in comparison with the two-dimensional mode growth in the reference case at zero-roughness height (e.g. figure 8).

3.3.2. *Evolution of f_Δ modes*

The above discussed results are restricted to the evolution of the three fundamental modes (f_{f1-3}), which have been excited upstream of the roughness element. In the following, the evolution of interaction modes, which are not excited in the flow by the disturbance source, but arise in the roughness wake is considered. In this context, figure 11 presents the spectral disturbance evolution for $h/\delta_{1,ref} = 0.3$ on the roughness centreline. The wall-normal distance is $y/\delta_{1,ref} = 0.9$, since the disturbances arising from the roughness interaction were observed to be most distinct close to that position (compare the last paragraph). Moreover, this position is very close to the critical layer, which is referred to as a thin layer enclosing the point, at which the

https://doi.org/10.1017/jfm.2014.499 Published online by Cambridge University Press

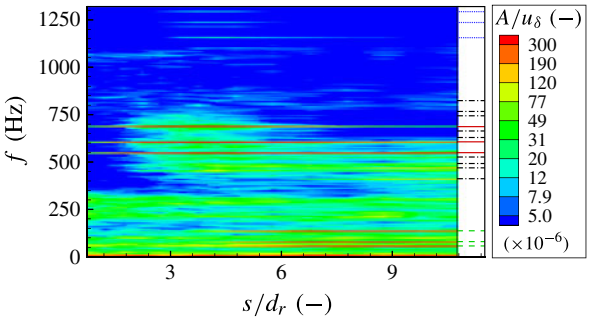


FIGURE 11. Spectral disturbance evolution on roughness centreline for $h/\delta_{1,ref} = 0.3$ (A at $y/\delta_{1,ref} = 0.9$, with frequencies of f_f, f_Δ, $f_{f,\Delta}$ and f_Σ indicated by solid (red), dashed (green), dash-dot (black) and dotted (blue) lines, respectively).

mean flow velocity equals the phase speed of the most distinct TS waves. In figure 11, the distinct peaks at the fundamental mode frequencies $f_{f1\text{–}3}$ are immediately apparent (indicated with a solid (red) line at the right). Parts of the low-frequency spectrum ($f = 0$–350 Hz) are affected by background noise and/or vibrations of the hot-wire traverse, which hinder the evaluation of low-amplitude, low-frequency boundary layer disturbance modes. This disturbing influence becomes also obvious in the reference spectrum for $h/\delta_{1,ref} = 0$ without controlled disturbance excitation in figure 8(*a*), but for a more detailed discussion the reader is referred to Plogmann *et al.* (2012*a*). Despite the spectral peaks for the fundamental mode frequencies, three distinct peaks are obvious in the low-frequency range ($f < 150$ Hz), in which TS waves are stable in the undisturbed boundary layer ($h/\delta_{1,ref} = 0$). These peaks are present at difference frequencies of the fundamental modes, that is, $f_{\Delta 21} = f_{f2} - f_{f1}$, $f_{\Delta 32} = f_{f3} - f_{f2}$ and $f_{\Delta 31} = f_{f3} - f_{f1}$ (indicated with dashed (green) lines at the right of figure 11). Hence, these low-frequency modes can be associated with the excited fundamental modes, but were not excited by the disturbance source and are, in the following, referred to as f_Δ modes.

Figure 12 shows the growth of the difference modes on the roughness centreline. Starting at $s/d_r > 2$, a continuous growth of the f_Δ modes can be observed. The growth is only weakly frequency dependent, similar as observed for the fundamental modes in the near wake (compare figure 8*a*). Due to an increased noise level in the low-frequency range (compare the last paragraph), the $f_{\Delta 21}$ mode can only be observed starting at $s/d_r = 4$. Far downstream ($s/d_r > 9$) the growth of the f_Δ modes levels off, before they are slightly damped. In the reference case the frequency bands of the f_Δ modes are dominated by noise (exemplarily shown for the mode $f_{\Delta 31}$ in figure 12). Hence, without roughness no significant growth of the f_Δ modes is present. The growth of the f_Δ modes downstream of the roughness can, therewith, be linked to the increased amplification of the fundamental modes in the near wake.

If the f_Δ modes arising in the roughness wake were a result of a wave interaction between two fundamental modes, one would also expect modes developing at the sum of the fundamental mode frequencies as for example at $f_{\Sigma 31} = f_{f1} + f_{f3}$ (in the following referred to as f_Σ modes). In the near wake an increased disturbance growth is observed for the f_Σ modes (as exemplarily shown for $f_{\Sigma 31} = 1235$ Hz in figure 12 and also obvious in figure 11). However, in contrast to the evolution of the f_Δ modes a growth of the f_Σ modes can only be observed for $s/d_r < 4$, whereas they are

https://doi.org/10.1017/jfm.2014.499 Published online by Cambridge University Press

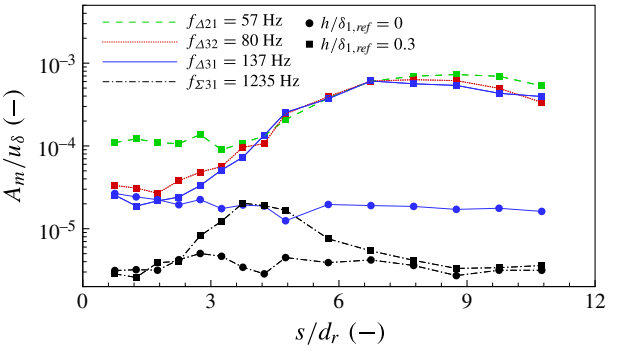


FIGURE 12. (Colour online) Streamwise amplitude evolution of f_Δ and f_Σ modes for $h/\delta_{1,ref} = 0.3$ on roughness centreline.

damped further downstream. Moreover, the f_Σ modes' amplitude is one to two orders of magnitude lower compared with the f_Δ modes' amplitude. Far downstream the amplitude of the f_Σ modes is even lower than the noise level (figure 11). Hence, although their amplitude is lower and the f_Σ modes are, therewith, regarded as less important in the transition process, the existence of the f_Σ modes supports the argument of a substantial wave interaction in between the fundamental modes in the roughness wake.

If the f_Δ and f_Σ modes were a result of a quadratic wave interaction of the fundamental modes, one would further expect that the amplitude evolutions were similar to the product of the fundamental modes' evolution. Figure 13 exemplarily shows the evolution for the product of the fundamental modes f_{f1} and f_{f3} and for the corresponding $f_{\Delta 31}$ and $f_{\Sigma 31}$ modes. For better comparison all distributions are normalized by their amplitude at $s/d_r = 3.75$. It is seen that the amplitude evolution of the f_Σ mode and the product of the fundamental modes correlate well in the entire measurement region. This gives strong evidence that the mechanism for the growth/decay of the f_Σ modes is a quadratic wave interaction of two fundamental modes. In contrast the f_Δ modes only show agreement for $s/d_r < 4$. Further downstream the growth of the f_Δ modes is increased compared with the quadratic wave interaction showing that another mechanism must be involved in the amplification of the f_Δ modes in the far wake.

Since the f_Δ modes significantly influence the disturbance growth in the roughness wake, a more detailed understanding of the f_Δ mode nature is attained in the following. Figure 14 shows the streamwise evolution of the wall-normal disturbance mode amplitude (*a*) and phase (*b*) distribution on the roughness centreline for the mode $f_{\Delta 31} = 137$ Hz. In the inner part of the boundary layer a peak in the f_Δ mode amplitude function is observed close to the critical layer ($y/\delta_{1,ref} = 0.8$–0.9). This position coincides with the peak, which was observed in the fundamental mode eigenfunction and could be attributed to the oblique ($\Theta \approx 45°$) modes arising as a result of the disturbance roughness interaction (see figure 8*b*). Comparing the disturbance mode amplitude function with the eigenfunction obtained by linear theory shows good agreement for the three-dimensional mode ($\Theta = 45°$, figure 14*a*). Smaller deviations are, however, obvious at $s/d_r = 4.75$. The comparison with the two-dimensional mode eigenfunction reveals larger deviations, especially in the outer part of the boundary layer ($y/\delta_{1,ref} > 3$). For the phase eigenfunction (figure 14*b*) a better consistency with the three-dimensional compared with the two-dimensional

https://doi.org/10.1017/jfm.2014.499 Published online by Cambridge University Press

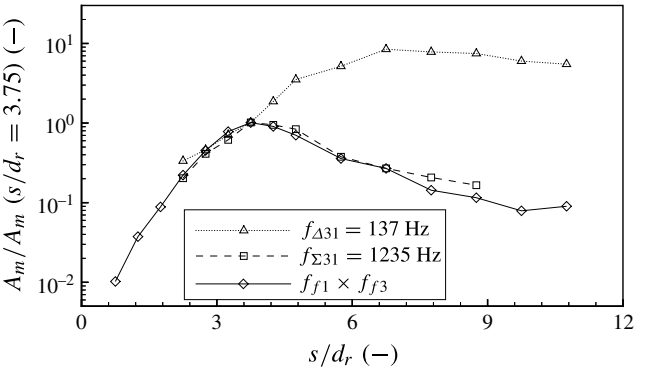


FIGURE 13. Streamwise amplitude evolution of $f_{\Delta 31}$, $f_{\Sigma 31}$ and $f_{f1} \times f_{f3}$ modes for $h/\delta_{1,ref} = 0.3$ on the roughness centreline.

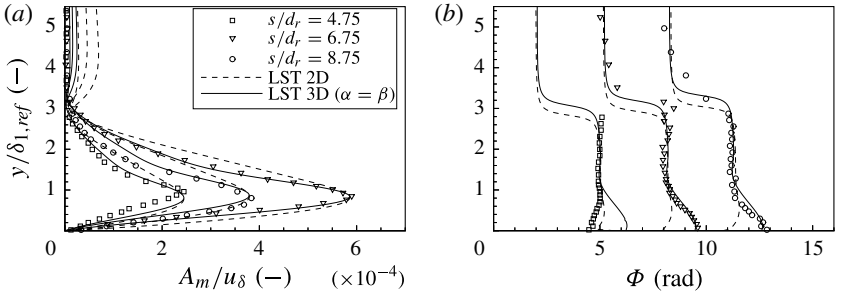


FIGURE 14. Wall-normal disturbance amplitude (*a*) and phase (*b*) function for $f_{\Delta 31} =$ 137 Hz mode at distinct streamwise positions on the roughness centreline for $h/\delta_{1,ref} = 0.3$, same legend for (*a*,*b*).

mode eigenfunction is confirmed despite in the near wake ($s/d_r = 4.75$), where a better agreement with the two-dimensional mode eigenfunction is present. Hence, the comparison with linear theory and with the fundamental mode evolution suggests a three-dimensional nature of the low-frequency interaction modes observed in the far roughness wake.

The spanwise nature of the low-frequency modes is further addressed in figure 15, which presents the streamwise development of the spanwise disturbance amplitude distribution (*a*) and of the corresponding spanwise wavenumber spectra (*b*) for the mode $f_{\Delta 31} = 137$ Hz. In compliance with the evolution of the fundamental modes (figures 9 and 10) the wall-normal distance is $y/\delta_{1,ref} = 0.9$. Based on the amplitude distribution (figure 15*a*) it is seen that the low-frequency modes start to grow in the centreline region and spread outwards in the streamwise evolution. The comparison with the amplitude distribution of the fundamental mode at $s/d_r = 5.75$ (indicated by a dashed line) reveals that the spread in spanwise direction is limited by the outer minima in the amplitude distribution of the fundamental mode. Moreover, the comparison with the fundamental mode suggests smaller-scale spanwise structures arising for the f_Δ modes. This observation is confirmed in the spanwise wavenumber spectra, as spanwise structures are present for $\pi < \beta d_r < 5\pi$ (figure 15*b*). This gives further evidence for a strong three-dimensional nature of the f_Δ modes. Moreover, the spanwise structures of the f_Δ modes persist far downstream in contrast to a

https://doi.org/10.1017/jfm.2014.499 Published online by Cambridge University Press

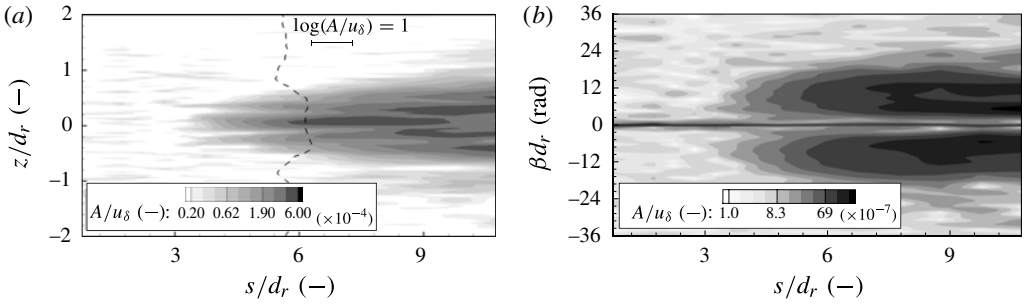


FIGURE 15. Disturbance mode evolution in the streamwise–spanwise plane (*a*) and corresponding spanwise wavenumber spectra (*b*) for $f_{\Delta 31} = 137$ Hz and $h/\delta_{1,ref} = 0.3$ at $y/\delta_{1,ref} = 0.9$ (fundamental mode distribution of $f_{f1} = 549$ Hz at $s/d_r = 5.75$ indicated by dashed line in (*a*)).

considerable damping of the three-dimensional structures observed for the fundamental mode (compare e.g. figure 10). The spanwise structures of the other two f_Δ modes ($f_{\Delta 21}$ and $f_{\Delta 32}$, not shown) are very similar as also hinted at by their evolution on the centreline (compare figure 12).

The above discussed results showed that the shape of the wall-normal disturbance mode function of the low-frequency f_Δ modes is similar to the characteristics predicted with linear theory. However, the distinct growth of the f_Δ modes in the far roughness wake is opposed to linear theory, based on which these modes are stable. Moreover, the f_Δ mode growth may only in a first instant be attributed to a quadratic wave interaction of the excited fundamental modes. Further downstream, however, another dominant mechanism seems to exist for the amplification of the f_Δ modes. The f_Δ mode characteristics show similarities to the theoretical (Wu *et al.* 2007) and recent experimental observations by de Paula *et al.* (2013) (compare § 1). However, in these theoretical and experimental studies the boundary layer is not exposed to a roughness element. The observations in the present experiment show, that the roughness element acts as an (additional) amplifier for the excited fundamental TS wave modes in the near roughness wake. Moreover, oblique modes are generated at the fundamental mode frequencies by the scattering of the initially two-dimensional TS waves at the roughness. Further downstream the mean flow relaxes towards a uniform state and also the linear stability characteristics are recovered for the fundamental modes. Therefore, it seems appropriate to compare the present experimental results at least in the far roughness wake to the previous theoretical (Wu *et al.* 2007) and experimental (de Paula *et al.* 2013) findings. The experiments by de Paula *et al.* (2013) confirm the present observations, in that the shape of the f_Δ modes compares well with linear theory for three-dimensional modes. Moreover, the f_Δ mode growth corresponded in a first stage to a quadratic wave interaction of the fundamental modes prior to a second nonlinear growth stage.

The phase-locked mechanism proposed by Wu *et al.* (2007) suggests an interaction between a two-dimensional (planar) and oblique TS modes, which share approximately the same phase speed, to be responsible for a super-exponential growth of f_Δ difference modes. In a first stage, the planar and oblique modes (at roughly the same phase speed) interact within their common critical layer. The interaction results in modes at difference and sum frequencies, for which an increased growth compared with linear theory is predicted for the f_Δ, whereas the f_Σ modes are restricted to the

https://doi.org/10.1017/jfm.2014.499 Published online by Cambridge University Press

critical layer. In agreement with the theoretical findings, it is seen that the disturbance growth downstream of the roughness is most distinct near the critical layer (figure 8, $y/\delta_{1,ref} = 0.8$–0.9). Moreover, the f_Δ modes in the present experiments exhibit a strong growth, whereas the sum modes are only very weakly pronounced (compare figures 11 and 12). The theoretical predictions further imply that in a first nonlinear stage only the growth behaviour of the f_Δ modes is affected, whereas the shape of the f_Δ mode eigenfunction is still dominated by linear characteristics. Hence, the good agreement of the f_Δ mode disturbance function with linear theory in the far roughness wake downstream of the roughness ($s/d_r > 4$, figure 14) suggests that the disturbance evolution in the present case mainly corresponds to the first (weakly) nonlinear stage.

The theoretical findings by Wu *et al.* (2007) are based on similar phase speeds for the two-dimensional and the oblique TS-modes. In that context, figure 16 shows the phase speeds of the two-dimensional and oblique modes occurring in the roughness wake, exemplarily for the fundamental mode f_{f1} and f_{f3} and the according $f_{\Delta 31}$ mode. The phase speeds are obtained at $s/d_r = 8.75$ based on linear theory, as the mean flow recovered the state of the undisturbed reference case at that streamwise location (see figure 8). Moreover, the growth rates of the fundamental modes compare well with the undisturbed reference case far downstream (see figure 8), so that the calculation of phase speeds based on linear theory seems reasonable. Figure 16 shows that 3D modes of the fundamental mode f_{f1} share approximately the same phase speed with the 2D fundamental mode f_{f3} near $\beta d_r = 4$. The corresponding difference mode $f_{\Delta 31}$ exhibits a similar phase speed in that particular spanwise wavenumber range. A comparison with the spanwise wavenumber spectrum of the $f_{\Delta 31}$ mode at this streamwise location (black line with squared symbols in figure 16) reveals that the most dominant spanwise modes are observed near $\beta d_r = 5$–6. Hence, there is a small difference in the spanwise wavenumber range, in which the most dominant f_Δ modes are observed on the one hand and in which the same phase speeds for the planar and oblique modes prevail on the other hand. Wu *et al.* (2007) state that a small mismatch in the phase speed of the planar and the oblique modes leads to an optimal growth for the f_Δ modes. In the present case, the most distinct spanwise f_Δ modes ($\beta d_r = 5$–6) would require a mismatch of 2–3 % between the phase speed of the two-dimensional $f_{f3} = 686$ Hz mode and the oblique modes of $f_{f1} = 549$ Hz. Following the discussion above, it is seen that there are strong hints in the present experiments for a phase-locked TS wave interaction, which could explain the nonlinear growth of f_Δ difference modes observed for $s/d_r > 4$ in figure 13.

In principle, the present observations could also be explained in the context of a subharmonic-type, frequency detuned resonance, since it was shown that resonant growth can still be observed for large-frequency detuned subharmonic modes (up to 90 % of the subharmonic frequency; compare e.g. Borodulin, Kachanov & Koptsev (2002*a*), Borodulin *et al.* (2002*b*)). Moreover, phase synchronism of the fundamental and the oblique modes is found in a wide spanwise wavenumber range around the exact subharmonic mode (spanwise wavenumber detuned resonance). This indicates that the concept of detuned subharmonic resonance and of phase-locked interactions are based on a similar physical mechanism. As the description by Wu *et al.* (2007) seems to have even less restrictions with regard to frequency and spanwise wavenumber of the low-frequency modes, the present results are in the following discussed in the context of the phase-locked interaction mechanism.

3.3.3. *Evolution of $f_{f,\Delta}$ modes*

The findings in § 3.3.2 suggest an interaction of the two-dimensional and the oblique fundamental modes in the roughness wake resulting in the growth of f_Δ modes, which

https://doi.org/10.1017/jfm.2014.499 Published online by Cambridge University Press

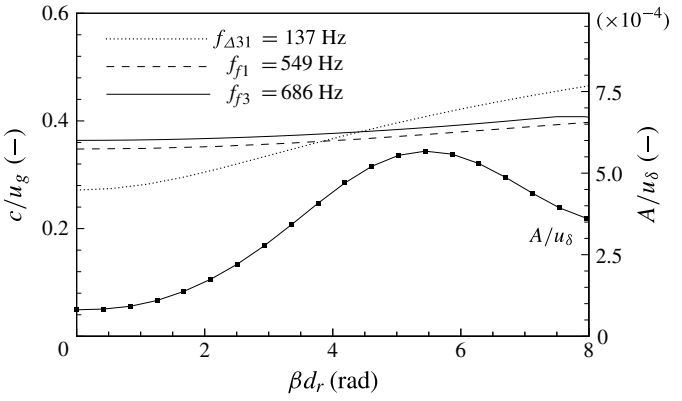


FIGURE 16. Phase speeds calculated with linear theory for f_{f1}, f_{f3} and $f_{\Delta 31}$ mode and spanwise wavenumber spectrum of $f_{\Delta 31}$ mode for $h/\delta_{1,ref} = 0.3$ at $s/d_r = 8.75$ and $y/\delta_{1,ref} = 0.9$.

Modes		Frequency	(Hz)
f_f (fund.) modes	f_{fi}	for $i = 1$–3	549, 606, 686
f_Δ modes	$f_{\Delta ij} = f_i - f_j$	for $ij = 21, 32, 31$	57, 80, 137
$f_{\Delta,\Delta}$ modes	$f_{\Delta,\Delta} = f_{\Delta 32} - f_{\Delta 21}, f_{\Delta 31} + f_{\Delta 21}, f_{\Delta 31} + f_{\Delta 32}$		23, 194, 217
$f_{f,\Delta}$ modes	$f_{f,\Delta} = f_{fi} \pm f_{\Delta kl}$	for $i = 1$–3 and $kl = 21, 32, 31$	412, 469, 492, 526, 629, 664, 744, 767, 824
f_h (har.) modes	$f_{hi} = 2f_{fi}$	for $i = 1$–3	1098, 1212, 1372
$f_{h,\Delta}$	$f_{h,\Delta} = f_{hi} \pm f_{\Delta kl}$	for $i = 1$–3 and $kl = 21, 32, 31$	961, 1019, 1041, ...

TABLE 2. Summary of disturbance mode frequencies with numerical values for f_m case (last column).

are in the following also referred to as primary wave interaction modes. Below, it is focused on secondary wave interaction modes, which are referred to as modes, which imply the interaction with a primary interaction mode. The spectral streamwise disturbance evolution (figure 11) reveals distinct peaks at frequencies $f_{f,\Delta}$, which hint at wave interactions between the fundamental modes and the primary interaction f_Δ modes. A summary of all secondary interaction modes that can theoretically be generated by an interaction of the fundamental (f_f) with the f_Δ modes can be found in table 2. In addition, these frequencies are indicated by a dash-dot line on the right-hand side of figure 11. The comparison with the indicated frequencies shows that in the experiment secondary wave interactions can only be observed in the lower-frequency range of possible interaction modes. This can likely be attributed to a less distinct growth/or even decay of the two higher-frequency fundamental modes (f_{f2} and f_{f3}) in the far wake (compare figure 8) so that nonlinear interactions with the f_Δ modes are less pronounced. Moreover, the higher-frequency secondary modes are damped based on linear theory, whereas the lower-frequency modes experience an amplification (compare figure 3).

Figure 17 shows the streamwise evolution of the wall-normal disturbance amplitude (*a*) and phase (*b*) function on the roughness centreline exemplarily for the secondary interaction mode $f_{f1,\Delta 31} = 412$ Hz. The most distinct peak in the amplitude function

https://doi.org/10.1017/jfm.2014.499 Published online by Cambridge University Press

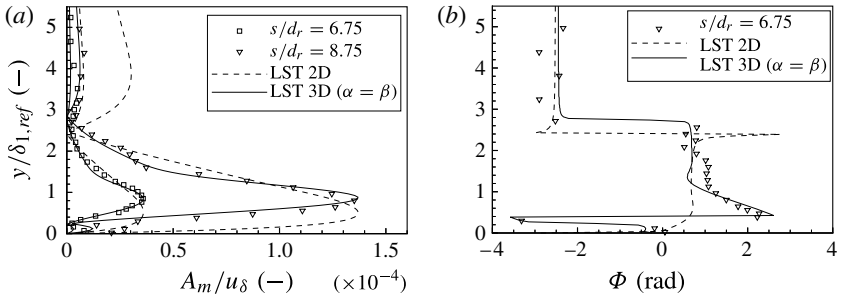


FIGURE 17. Wall-normal disturbance amplitude (*a*) and phase (*b*) function for $f_{f1,\Delta 31} = 412$ Hz mode at $h/\delta_{1,ref} = 0.3$ on roughness centreline.

(figure 17*a*) is observed near the critical layer ($y/\delta_{1,ref} \approx 0.9$) similar as observed for the f_Δ modes (compare figure 14). Comparing the wall-normal disturbance shape to eigenfunctions obtained with linear theory shows very good agreement for the three-dimensional mode ($\alpha = \beta$) both in the inner and outer region of the boundary layer. In contrast considerably larger deviations are present in relation to the two-dimensional mode eigenfunction. The phase distribution along the wall-normal coordinate is exemplarily shown at $s/d_r = 6.75$ (figure 17*b*), since the shape of the phase eigenfunction is only marginally affected in the streamwise evolution ($6 < s/d_r < 11$). The comparison with linear theory confirms that the experimental results correlate better with the three-dimensional compared with the two-dimensional mode eigenfunction especially in the near-wall region. Hence, the three-dimensional nature of the secondary interaction modes can be well described by linear theory within the measurement domain similar as observed for the primary interaction f_Δ modes (compare figure 14).

Below, the streamwise amplitude evolution of the secondary $f_{f,\Delta}$ interaction modes is, at first, related to the amplitude of the excited fundamental (f_f) modes and of the primary interaction (f_Δ) modes. Figure 18 shows the RMS amplitude of all modes belonging to a certain group (in the following denoted by a Σ). Accordingly, the fundamental mode amplitude is for example $\Sigma f_f = \sqrt{f_{f1}^2 + f_{f2}^2 + f_{f3}^2}$. In figure 18 it is seen that the fundamental modes are most distinct within the entire measurement domain. The primary (f_Δ) interaction modes can be observed starting at $s/d_r = 3$ and the growth levels off for $s/d_r > 7$. A growth of the $f_{f,\Delta}$ modes is already present for $s/d_r > 1$. However, compared with the fundamental modes the amplitude of the secondary interaction ($f_{f,\Delta}$) modes is one to two orders of magnitude lower in the near roughness wake. The comparison with figure 11 shows that distinct peaks at the $f_{f,\Delta}$ mode frequencies are not present in the near wake. The growth in the $f_{f,\Delta}$ mode frequency bands (figure 18) is rather connected to the naturally (not excited) arising disturbances in the near wake (compare figure 11), which are most distinct for $f = 400$–800 Hz. Hence, the natural disturbances arise in the same frequency range, in which the $f_{f,\Delta}$ modes are observed and, therewith, cause the $f_{f,\Delta}$ growth for $s/d_r < 6$ in figure 18. In contrast far downstream ($s/d_r > 8$), a second pronounced growth of $f_{f,\Delta}$ modes is now in compliance with distinct peaks at frequencies of the secondary wave interaction modes (compare figure 11). However, a comparison at the end of the measurement domain reveals that the $f_{f,\Delta}$ modes' amplitude is still an order of magnitude lower in relation to the fundamental mode amplitude.

https://doi.org/10.1017/jfm.2014.499 Published online by Cambridge University Press

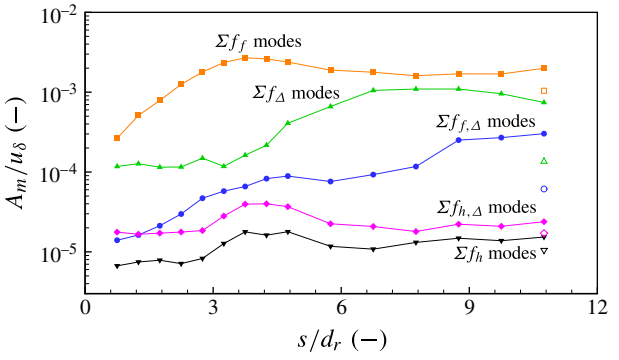


FIGURE 18. (Colour online) Streamwise amplitude evolution for Σf_f, Σf_Δ, $\Sigma f_{f,\Delta}$, Σf_h and $\Sigma f_{h,\Delta}$ modes on roughness centreline for $h/\delta_{1,ref} = 0.3$ (reference case $h/\delta_{1,ref} = 0$ indicated by open symbols at $s/d_r = 10.75$).

Figure 18 also includes the amplitude evolution of the (second) harmonic modes, which can be attributed to the excited fundamental modes. Accordingly, the harmonic modes (f_h) evolve with a similar characteristic as the fundamental modes, that is they grow/decay with the fundamental modes, however, at significantly lower amplitude. Therefore, they are most pronounced near $s/d_r = 4$, whereas they can hardly be distinguished from the noise level at the end of the measurement domain. Nevertheless, a wave interaction of the harmonic with the primary interaction f_Δ modes is observed at distinct frequencies $f_{h,\Delta}$ (see table 2). The $f_{h,\Delta}$ modes' streamwise evolution is very similar compared with the harmonic mode evolution, but their amplitude is slightly higher. However, in comparison with the fundamental and the other interaction modes (f_Δ, $f_{f,\Delta}$) the amplitude of the $f_{h,\Delta}$ modes is still marginal. Hence, for the transition process downstream of the roughness both the f_h and $f_{h,\Delta}$ modes are of minor importance.

Finally, the comparison with the reference case at $s/d_r = 10.75$ (indicated by open symbols in figure 18) shows that for none of the interaction modes (f_Δ, f_h, $f_{h,\Delta}$) developing downstream of the roughness a substantial growth is present in the reference case ($h/\delta_{1,ref} = 0$), except for $f_{f,\Delta}$. However, in that case the growth is associated with linear theory since the frequencies are within the range of the most convectively amplified disturbances (compare figure 3). Therefore, in the reference case the disturbance growth is clearly dominated by the linear growth of the fundamental modes, whereas in the roughness wake a nonlinear growth of primary (f_Δ) and secondary ($f_{f,\Delta}$) interaction modes prevails in addition to the fundamental mode growth.

In the following, the growth of the $f_{f,\Delta}$ modes is further investigated, as the preceding discussion showed that these modes are the most distinct secondary wave interaction modes. Figure 19 shows the amplification of the mode $f_{f1,\Delta 31} = 412$ Hz, which can be observed for $s/d_r > 5.75$. Moreover, the growth according to linear theory for a two-dimensional and three-dimensional mode and the product of the fundamental mode f_{f1} and the $f_{\Delta,31}$ mode are indicated in figure 19. For better comparison, all evolutions are normalized by their amplitude at $s/d_r = 5.75$. Comparing the $f_{f1,\Delta 31}$ mode evolution with linear theory shows that the growth is increased significantly and cannot be predicted based on linear theory (neither for the two- nor for the three-dimensional mode). Moreover, the growth expected for

https://doi.org/10.1017/jfm.2014.499 Published online by Cambridge University Press

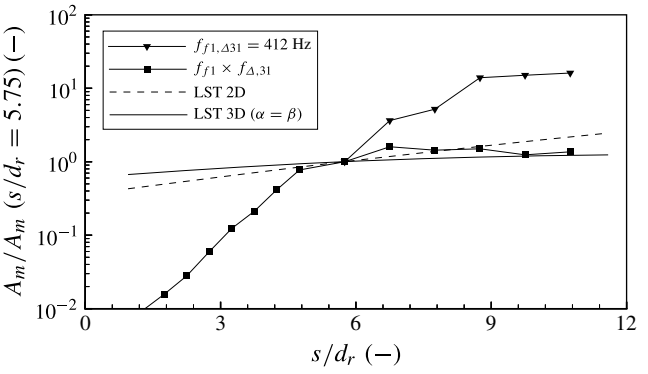


FIGURE 19. Streamwise amplitude evolution of $f_{f1,\Delta31}$, $f_1 \times f_{\Delta31}$ and $f_{LST} = 412$ Hz (two- and three-dimensional) mode on the roughness centreline.

a quadratic wave interaction of the fundamental with the $f_{\Delta,31}$ mode (represented by the product $f_{f1} \times f_{f1,\Delta31}$) does also show considerably smaller growth rates than observed for the $f_{f1,\Delta31}$ mode. Hence, similar as observed for the primary interaction modes, the growth of the secondary $f_{f,\Delta}$ interaction modes cannot be explained by linear theory nor by a quadratic wave interaction. Nevertheless, the shape of the disturbance function is in good agreement with results predicted by linear theory (compare figure 17).

Below, it is analysed whether the phase-locked interaction mechanism, which is a reasonable explanation for the strong growth of the f_Δ modes, can also cause the growth of the secondary interaction modes. In that context, the phase speeds (obtained with linear theory) for the respective modes at $s/d_r = 8.75$ and the corresponding spanwise wavenumber spectrum of the mode $f_{f1,\Delta31}$ are depicted in figure 20. For the two-dimensional mode $f_{f1} = 549$ Hz and the oblique modes of $f_{\Delta31} = 137$ Hz similar phase speeds are present close to $\beta d_r = 4$. The most distinct spanwise modes of the resulting interaction mode $f_{f1,\Delta31}$ are observed near $\beta d_r = 6$. For $\beta d_r = 6$ the mismatch in the phase speeds for the two-dimensional fundamental f_{f1} and the oblique $f_{\Delta31}$ modes is 21 % due to a strong dependency of the f_Δ mode phase speed on the spanwise wavenumber. An order of magnitude analysis by Wu *et al.* (2007) suggests that a phase-speed mismatch of $O(\sigma^2)$ can still result in an optimal growth of difference modes. Applying this to the present experiments gives $\sigma^2 = Re_{\delta1}^{-1/5} = 22\,\%$. Hence, the phase-locked interaction mechanism might also explain the strong amplification of the secondary $f_{f,\Delta}$ interaction modes in the far roughness wake. Moreover, in figure 20 it is apparent that the oblique modes of f_{f1} and $f_{f1,\Delta31}$ have the same phase speeds near the spanwise wavenumber $\beta d_r = 6$, for which the most distinct oblique modes of $f_{f1,\Delta31} = 412$ Hz (black line with symbols in figure 20) are observed.

Finally, the streamwise–spanwise evolution of the secondary interaction ($f_{f,\Delta}$) modes is shown in more detail in figure 21 at $y/\delta_{1,ref} = 0.9$ (close to the critical layer). It is seen that the growth most distinctively begins in the centreline region and that the disturbance mode spreads outwards in the streamwise evolution. Similarly as observed for the primary interaction modes (see figure 15) the spanwise extend seems to be limited by the outer minima in the fundamental mode evolution, which is indicated at $s/d_r = 8.75$ (dashed line in figure 21*a*). In the spanwise wavenumber spectra (figure 21*b*), a continuous growth of oblique modes, which are most distinct near

https://doi.org/10.1017/jfm.2014.499 Published online by Cambridge University Press

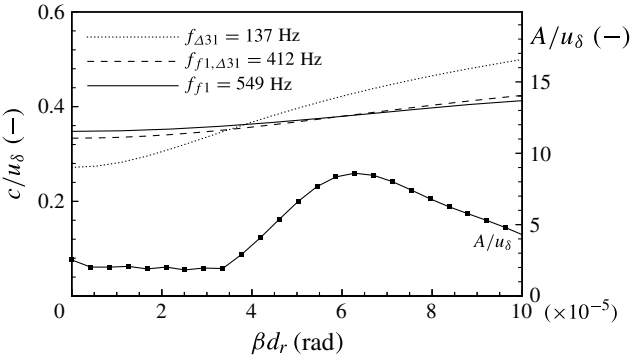


FIGURE 20. Phase speeds calculated with linear theory for f_{f1}, $f_{\Delta 31}$ and $f_{f1,\Delta 31}$ mode and spanwise wavenumber spectrum of $f_{f1,\Delta 31}$ mode for $h/\delta_{1,ref} = 0.3$ at $s/d_r = 8.75$ and $y/\delta_{1,ref} = 0.9$.

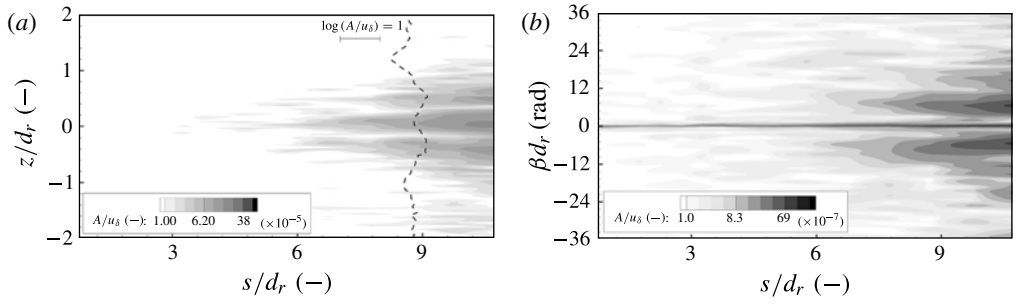


FIGURE 21. Disturbance mode evolution (*a*) and corresponding spanwise wavenumber spectra (*b*) for $f_{f1,\Delta 31} = 412$ Hz in the streamwise–spanwise plane at $y/\delta_{1,ref} = 0.9$ for $h/\delta_{1,ref} = 0.3$ (fundamental mode distribution of $f_{f1} = 549$ Hz at $s/d_r = 8.75$ indicated by dashed line in (*a*)).

$\beta d_r = 6$, confirm the three-dimensional nature of the secondary wave interaction ($f_{f,\Delta}$) modes that was already hinted at in the comparison of the wall-normal disturbance function with linear theory (see figure 17). Moreover, in the streamwise evolution a growth of smaller-scale spanwise modes is present, in contrast to the fundamental mode evolution, for which the three-dimensional structures are damped in the far wake (compare e.g. figure 10).

3.4. *Influence of roughness height*

The above-presented results for the wave interaction modes in the roughness wake referred to a roughness height of $h/\delta_{1,ref} = 0.3$. Below, the disturbance growth in the roughness wake is discussed with respect to the influence of the roughness height in the medium height range, that is four discrete roughness heights have been investigated ($h/\delta_{1,ref} = [0.2, 0.3, 0.4, 0.5]$). These roughness heights correspond to roughness Reynolds numbers of $Re_h = [30, 70, 125, 195]$, respectively. Without controlled disturbance excitation upstream of the roughness, the mean flow evolution is qualitatively similar in this roughness height range (compare figures 6 and 7).

At first, figure 22 depicts the spectral disturbance evolution in the roughness wake for $h/\delta_{1,ref} = 0.4$ similar as shown in figure 11 for a roughness height of $h/\delta_{1,ref} = 0.3$.

https://doi.org/10.1017/jfm.2014.499 Published online by Cambridge University Press

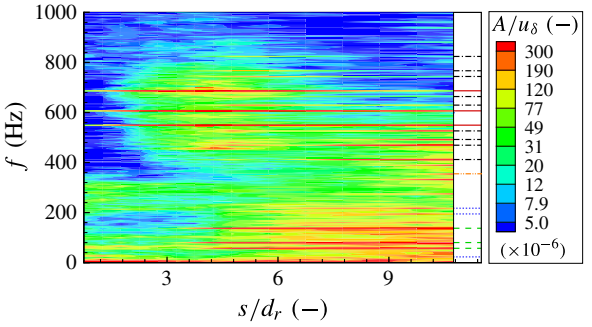


FIGURE 22. Spectral disturbance evolution on roughness centreline for $h/\delta_{1,ref} = 0.4$ (A at $y/\delta_{1,ref} = 0.9$, with frequencies of f_f, f_Δ, $f_{\Delta,\Delta}$, $f_{f,\Delta}$ and f_{ter} indicated in solid (red), dashed (green), dotted (blue), dash-dot (black) and dash-dotdot (orange) lines respectively).

Comparing the disturbance evolutions reveals a considerably increased growth of the fundamental (f_f) modes and, consequently, of the primary (f_Δ) and secondary ($f_{f,\Delta}$) interaction modes with the roughness height. Therefore, for $h/\delta_{1,ref} = 0.4$ the $f_{f,\Delta}$ modes can also be observed in the high-frequency range ($500 < f < 800$ Hz). However, far downstream the higher-frequency $f_{f,\Delta}$ modes are only weakly distinct, since the fundamental mode f_{f3} is damped with the relaxation of the mean flow. Hence, in the far wake, the $f_{f,\Delta}$ modes are more dominant in the low-frequency range ($400 < f < 600$ Hz) in compliance with findings for $h/\delta_{1,ref} = 0.3$.

In the far wake at $h/\delta_{1,ref} = 0.4$, a disturbance growth is present at distinct frequencies $f_{\Delta,\Delta}$ (indicated by a dotted (blue) line in figure 22, see also table 2) hinting at self-interactions in between the f_Δ modes. Within the measurement domain ($s/d_r < 11$), self-interactions were not observed for $h/\delta_{1,ref} = 0.3$ and the comparison with linear stability characteristics (figure 3) shows that the secondary $f_{\Delta,\Delta}$ modes are stable in the undisturbed reference case ($h/\delta_{1,ref} = 0$). According to Wu *et al.* (2007) self-interactions of the oblique modes occur in a third nonlinear stage, in which these self-interactions can become as important as the phase-locked wave interaction (further addressed below). The growth behaviour of the $f_{\Delta,\Delta}$ modes is addressed in figure 23(a) for $h/\delta_{1,ref} = 0.4$. The amplitude evolutions are normalized by the respective amplitude at $s/d_r = 5.75$. The quadratic wave interaction between the respective primary wave interaction modes is indicated by their amplitude product ($f_{\Delta 31} \times f_{\Delta 32}$). Within the measurement domain, good agreement between the amplitude product of the primary interaction modes and the growth behaviour of the $f_{\Delta 31,\Delta 32}$ mode is observed. Hence, the growth of the secondary $f_{\Delta,\Delta}$ interaction modes can, at first, likely be attributed to a quadratic wave interaction between the primary interaction modes.

In the spectral disturbance evolution downstream of the roughness at $h/\delta_{1,ref} = 0.4$ (figure 22) further distinct frequency peaks are present. The frequencies of these peaks hint at tertiary wave interactions, which are referred to as wave interactions between a secondary and another (fundamental, primary, secondary) disturbance mode. Hence, these modes can theoretically be generated in a wide frequency range, but are most distinct in the low-frequency range ($f < 400$ Hz). Exemplarily, a tertiary wave interaction is indicated in figure 22 for $f_{ter} = f_{f1,\Delta 31} - f_{\Delta 32} = 412 - 57 = 355$ Hz. The growth of this particular mode is depicted in figure 23(b). The comparison with linear theory shows good agreement for $s/d_r < 4$ in a first stage, whereas the amplification

https://doi.org/10.1017/jfm.2014.499 Published online by Cambridge University Press

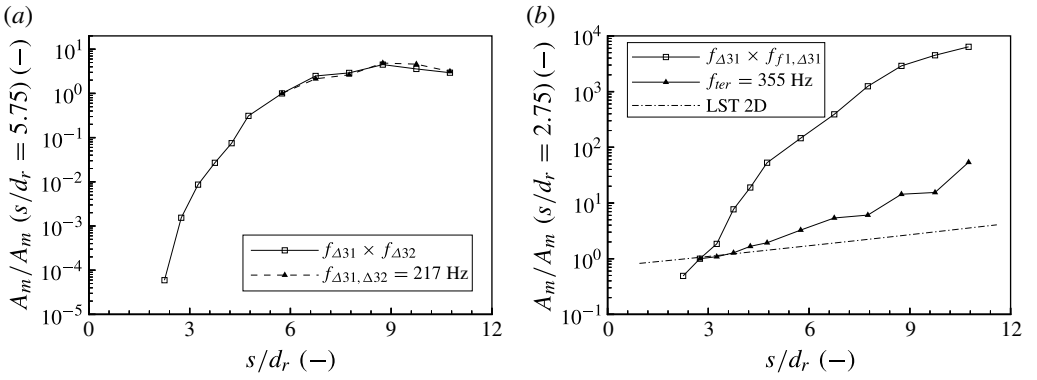


FIGURE 23. Streamwise amplitude evolution of $f_{\Delta31,\Delta32}$ mode and $f_{\Delta31} \times f_{\Delta32}$ (a) and of f_{ter} mode and $f_{\Delta31} \times f_{f1,\Delta31}$ (b) for $h/\delta_{1,ref} = 0.4$ on roughness centreline.

is weakly nonlinear further downstream, but still less distinct as expected for a quadratic wave interaction of the $f_{\Delta31}$ and the $f_{f1,\Delta31}$ mode. Nevertheless, the growth of these tertiary interaction modes for $h/\delta_{1,ref} = 0.4$ leads to an increasing part of the disturbance spectrum in the far wake, which is affected by discrete frequency disturbance modes. Hence, the disturbance level especially in the low-frequency range is substantially increased for $h/\delta_{1,ref} = 0.4$ (figure 22) in comparison with $h/\delta_{1,ref} = 0.3$ (figure 11) finally leading to a shift in the transition location.

In the following, figure 24 in connection with figure 18 summarizes the evolution of the most distinct disturbance modes, that is fundamental, primary interaction (f_Δ) and secondary interaction ($f_{\Delta,\Delta}$ and $f_{f,\Delta}$) modes in the roughness wake for medium roughness heights, that is $h/\delta_{1,ref} = [0.2, 0.3, 0.4, 0.5]$. In figure 24 the RMS amplitude for all modes belonging to a certain group is depicted (compare also figure 18). For $h/\delta_{1,ref} = 0.2$ (figure 24a), only the fundamental mode evolution is noticeably affected by the disturbance roughness interaction, whereas the amplitude in the frequency bands of the interaction modes is hardly increased compared with the reference case ($h/\delta_{1,ref} = 0$, dashed lines). In compliance with the observations for $h/\delta_{1,ref} = 0.3$ (figure 8a), similar growth rates for the fundamental modes are observed (compared with the reference case) when the boundary layer recovered from the roughness interaction ($s/d_r > 7$). Hence, for $h/\delta_{1,ref} \leqslant 0.3$ the disturbance evolution is dominated by the growth of the fundamental modes within the measurement domain. In contrast, for $h/\delta_{1,ref} \geqslant 0.4$ the growth of the interaction modes is increased so that for $s/d_r > 6$ the disturbance evolution is dominated by the f_Δ modes. Moreover, the comparison with $h/\delta_{1,ref} = 0.5$ shows, that especially the growth of the low-frequency interaction modes (f_Δ and $f_{\Delta,\Delta}$) substantially increases with the roughness height and, finally, trips turbulence (as argued below).

From the discussion above, it is obvious that the evolution of the lower-frequency interaction modes is essential with regard to the disturbance evolution in the far roughness wake for $h/\delta_{1,ref} \geqslant 0.4$. Figure 25 shows the different growth stages of the f_Δ modes exemplarily for the mode $f_{\Delta31}$. The development of a quadratic wave interaction (represented by the product of the respective fundamental modes f_1 and f_3) is presented for reference. For $h/\delta_{1,ref} \geqslant 0.3$ the amplitude evolutions are normalized by the respective amplitude at $s/d_r = 3.25$, since the amplitude upstream ($s/d_r < 2.5$) is lower than the electronic noise floor in the case of $h/\delta_{1,ref} = 0.3$. For $h/\delta_{1,ref} \geqslant 0.3$, the f_Δ mode evolution matches the product of the fundamental modes for $s/d_r < 4$.

https://doi.org/10.1017/jfm.2014.499 Published online by Cambridge University Press

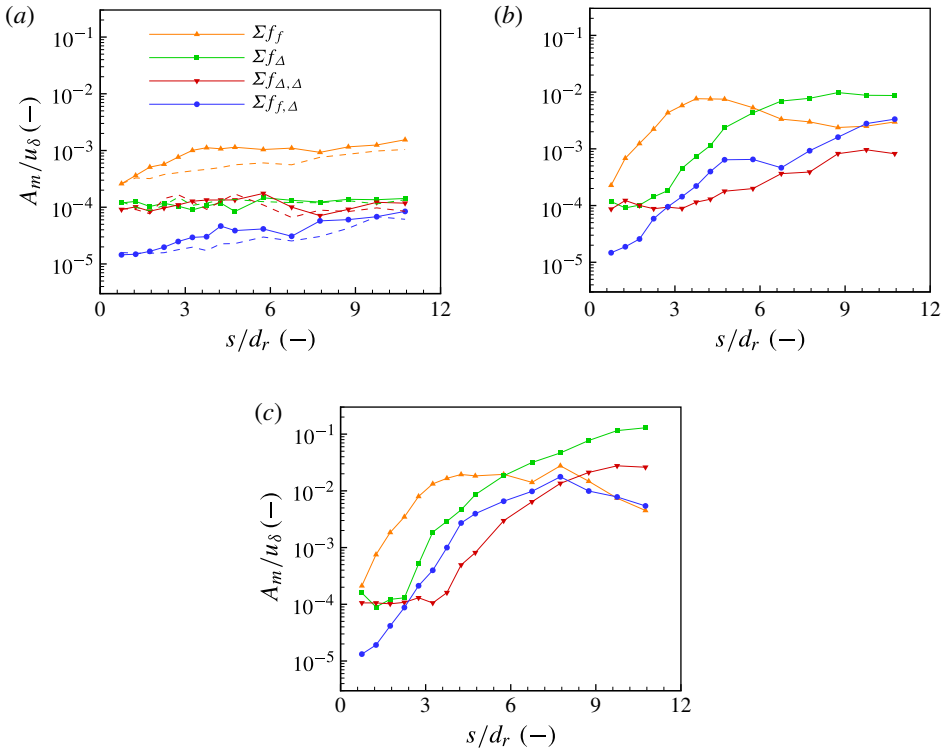


FIGURE 24. (Colour online) Streamwise evolution of fundamental (Σf_f), primary interaction (Σf_Δ) and secondary interaction ($\Sigma f_{\Delta,\Delta}$ and $\Sigma f_{f,\Delta}$) modes on the roughness centreline for $h/\delta_{1,ref} = 0.2$ (with reference case $h/\delta_{1,ref} = 0$ indicated by dashed lines) (*a*), $h/\delta_{1,ref} = 0.4$ (*b*) and $h/\delta_{1,ref} = 0.5$ (*c*), same legend for (*a–c*).

This confirms previous observations, in that the growth of the f_Δ modes in the near wake can well be described by a quadratic wave interaction of the fundamental modes. In the streamwise evolution, the growth behaviour of the fundamental and the primary f_Δ interaction modes starts to differ when the local maximum of the fundamental mode amplitude is reached at $s/d_r = 4$. Further downstream the fundamental modes are damped with the relaxation of the mean flow (see also figure 8*a*). In contrast, the primary f_Δ interaction modes enter a second nonlinear growth stage, which has been associated with the phase-locked interaction mechanism (see § 3.3.2). Hence, for $h/\delta_{1,ref} \geqslant 0.3$ transition from the first to the second nonlinear growth stage of the f_Δ modes is linked to the local maximum of the fundamental modes in the near wake, which appears rather independent of the streamwise coordinate within the medium roughness height range at $s/d_r \approx 4$. Finally, for $h/\delta_{1,ref} = 0.2$, the primary wave interaction (f_Δ) modes are only very weakly pronounced in the far roughness wake. Therefore, the amplitude evolutions for $h/\delta_{1,ref} = 0.2$ are normalized at $s/d_r = 7.75$ showing good agreement in the measurement region. Hence, a second nonlinear stage is not present within the measurement region ($s/d_r < 11$) for $h/\delta_{1,ref} = 0.2$.

Below, further light is shed on the nonlinear growth stages of the f_Δ modes. For $h/\delta_{1,ref} = 0.3$, it was seen that in the second nonlinear stage (downstream of $s/d_r = 4$) mainly the amplitude, but not the disturbance mode eigenfunction was affected (compare § 3.3.2). In contrast, for $h/\delta_{1,ref} = 0.5$ the comparison with linear

https://doi.org/10.1017/jfm.2014.499 Published online by Cambridge University Press

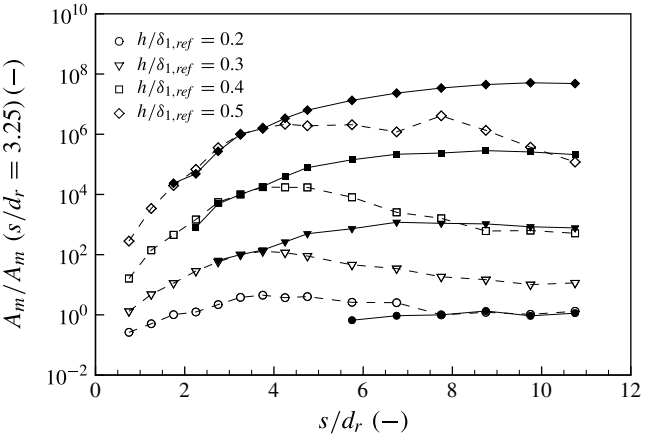


FIGURE 25. Streamwise amplitude evolution of $f_{\Delta 31}$ mode (solid lines with filled symbols) and $f_{f1} \times f_{f3}$ (dashed lines with open symbols) for different roughness heights on roughness centreline (shifted by 2 decades per $\Delta h/\delta_{1,ref} = 0.1$).

theory for a three-dimensional mode reveals that the modal shape is also disturbed shortly downstream of $s/d_r = 4$ (figure 26). In the streamwise evolution, the peak in the disturbance function is shifted off the wall, so that the mismatch with regard to the linear eigenfunction is rapidly increasing. Within the concept of phase-locked interactions a nonlinear stage II was proposed, in which not only the amplitude but also the shape of the eigenfunction is affected. At first, a thickening in the region of the disturbance maximum is observed compared with the modal disturbance shape, whereas the peak position is hardly affected. In the present experiments a small thickening in the disturbance function can be observed in the near-wall region ($y/\delta_{1,ref} < 0.6$) at $s/d_r = 4.75$, however, the peak is already significantly shifted off the wall at this streamwise location. Wu *et al.* (2007) state that their second nonlinear stage is weakly distinct in case the disturbance amplitude of the oblique modes is not sufficiently small, which might apply to the present case with $h/\delta_{1,ref} = 0.5$, for which a strong growth of the f_Δ modes is already observed in the near roughness wake (compare figure 24*c*). In that case, the disturbances enter a fully nonlinear stage, in which self-interactions between the f_Δ become pronounced. Moreover, the peak in the disturbance eigenfunction can be shifted considerably off the wall, as observed in figure 26. In the present experiments, self-interactions ($f_{\Delta,\Delta}$ modes) are observed starting at $s/d_r > 4$ (figure 24*c*) in compliance with the beginning deformation of the modal shape at $s/d_r = 4.75$ (figure 26). Hence, for the disturbance evolution in the far wake of the roughness at $h/\delta_{1,ref} = 0.5$ similarities to the late nonlinear stages described within the concept of phase-locked interactions are obvious.

In the following, the influence of the roughness height on the oblique modes generated by the disturbance roughness interaction is considered. At first, figure 27 shows a comparison of the fundamental mode f_{f1} spanwise structures arising in the roughness wake for $h/\delta_{1,ref} = 0.3$ and $h/\delta_{1,ref} = 0.5$. In the near wake ($s/d_r < 4$) the spanwise structures are qualitatively similar, but more pronounced for $h/\delta_{1,ref} = 0.5$ compared with those for $h/\delta_{1,ref} = 0.3$. In the streamwise evolution minima develop in the outer spanwise region, in between which the most dominant structures arising from the disturbance roughness interaction are observed. In comparison with $h/\delta_{1,ref} = 0.3$ it is seen that the minima are more distinct and spread further

https://doi.org/10.1017/jfm.2014.499 Published online by Cambridge University Press

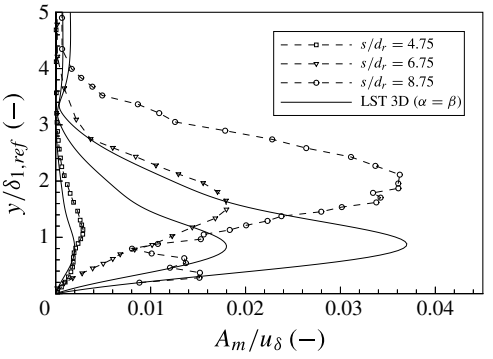


FIGURE 26. Wall-normal disturbance amplitude function for $f_{\Delta 31} = 137$ Hz mode at distinct streamwise positions on roughness centreline for $h/\delta_{1,ref} = 0.5$.

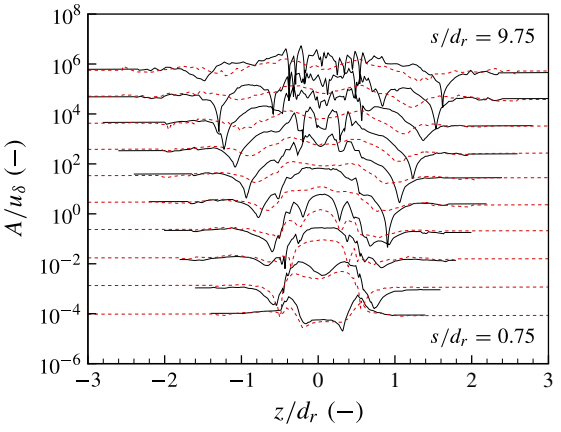


FIGURE 27. (Colour online) Evolution of fundamental mode f_{f1} in the streamwise–spanwise plane for $h/\delta_{1,ref} = 0.3$ (dashed) at $y/\delta_{1,ref} = 0.9$ and for $h/\delta_{1,ref} = 0.5$ (solid) at $y/\delta_{1,ref} = 1.0$ (shifted by one decade per $\Delta s/d_r = 1$).

outwards for $h/\delta_{1,ref} = 0.5$. Hence, the spanwise interaction domain, in which the disturbance evolution is affected downstream of the roughness, is increased with the roughness height. Moreover, opposed to $h/\delta_{1,ref} = 0.3$ a damping of the spanwise structures excited by the roughness element in the far wake cannot be observed for $h/\delta_{1,ref} = 0.5$. Instead, the substantially increased growth of the spanwise fundamental modes in the near wake results in the occurrence of smaller-scale spanwise structures in the centreline region. Hence, larger wave-type modes breakdown into smaller-scale spanwise structures, which is associated with the onset of turbulence. Within the measurement domain, the growth of these small-scale structures and, therewith, the onset of turbulence is, at first, restricted to $z/d_r \approx \pm 0.5$ (compare figure 27).

Below, more details of the spanwise disturbance evolution are obtained from the spanwise wavenumber spectra for $h/\delta_{1,ref} = 0.5$, which are depicted at selected streamwise positions in a frequency range $f < 1000$ Hz. In figure 28 averaged (with respect to $\pm\beta$) spectra are shown, since the disturbance evolution in the roughness wake is symmetric with respect to the centreline (compare e.g. figure 27). The comparison with the fundamental mode evolution at $h/\delta_{1,ref} = 0.3$ shows agreement

https://doi.org/10.1017/jfm.2014.499 Published online by Cambridge University Press

in the following observations. At first, the energy of the local peaks in the spanwise disturbance distribution directly downstream of the roughness is spread into a broad range of spanwise modes (figure 28*a*). Second, oblique (fundamental) modes are most pronounced near $\beta d_r = 2\pi$ in the near wake (figure 28*b*) confirming that the dominant spanwise wavelengths are in the same range as the streamwise wavelength of the fundamental modes. Moreover, in the near wake pronounced f_Δ modes are present for $\pi < \beta d_r < 5\pi$. However, due to the increased growth of the fundamental and the subsequent interaction modes the disturbance evolution in the far wake differs significantly. That is, in the streamwise evolution ($s/d_r = 6.75$, figure 28*c*) more energy is contained in smaller-scale spanwise wavenumber modes, especially for the fundamental and the f_Δ modes. Moreover, the growth of the fundamental and the subsequent (primary, secondary and tertiary) wave interaction modes progressively fills up the disturbance spectrum. Hence, far downstream (figure 28*d*) the spectrum takes on a turbulent character especially in the high-frequency range. Dominant spanwise modes, which are well above the broadband level of the turbulent spectrum, are still obvious in the low-frequency range ($f < 200$ Hz). Hence, the low-frequency modes reach higher amplitudes before the breakdown is initiated and subsequently the energy is spread into spanwise broadband modes (compare also figure 24*c*). This gives further evidence for the substantial meaning of the low-frequency interaction modes in causing turbulence in the wake of medium height roughness elements.

Finally, the strong growth of the disturbance modes for $h/\delta_{1,ref} = 0.5$ does also affect the mean flow evolution predominately in the far wake (figure 29). In the near wake high- and low-speed streaks are present hinting at the formation of two counter-rotating vortex pairs similar as observed for $h/\delta_{1,ref} = 0.3$, but the streaks have a higher amplitude for $h/\delta_{1,ref} = 0.5$. Further downstream ($s/d_r > 5$) the growth of additional high-speed streaks is seen at $z/d_r = \pm 0.25$. In contrast to the initial streaks at $z/d_r = \pm 0.5$, these streaks are growing in the far wake and reach an amplitude of 27 % of the local velocity corresponding to 13 % of the velocity at the boundary layer edge. Hence, the secondary high-speed streaks are significantly more pronounced in the far wake compared with the primary vortical structures arising in the near wake. The growth of the high-speed streaks together with the observed low-speed streaks at the edges of the high-speed streaks suggests the formation of secondary vortical structures as indicated in figure 29 in the far wake. Moreover, at the end of the measurement domain the mean flow velocity in the centreline region increases in a last step towards a fully turbulent boundary layer only less further downstream.

The spanwise distribution of the integral streamwise velocity fluctuations (contour levels in figure 29) shows that the disturbance roughness interaction is restricted to the spanwise roughness size in the near wake ($s/d_r < 4$). Further downstream the spanwise interaction domain increases and a wedge-shaped region with distinct fluctuations is observed. Moreover, a formation of lobes with maximum disturbance intensity u' becomes obvious. The spanwise position of these lobes seems to coincide with regions of high spanwise shear, as can be deduced from the comparison with the spanwise mean flow velocity distribution. Hence, in the late stages of transition, a disturbance growth in spanwise local shear layers might also contribute to the broadband disturbance character of the boundary layer spectrum, similar as observed in the experiments by Ergin & White (2006). However, the secondary high-speed streaks and the evolving spanwise shear stresses are clearly a consequence of the strong disturbance growth of the fundamental and the involved combination modes in the near roughness wake, which are in turn regarded the dominant source in triggering turbulence in the present study.

https://doi.org/10.1017/jfm.2014.499 Published online by Cambridge University Press

3.5. *The influence of disturbance frequency*

The most distinct disturbance modes that arise naturally (without controlled disturbance excitation) in the near wake of the roughness are observed for $f = 400$–750 Hz (see figures 11 and 30). Note that parts of the low-frequency spectrum ($f < 350$ Hz) are affected by background noise and/or vibrations of the hot-wire traverse (compare discussion of figure 11). Hence, the above discussed fundamental modes ($f_{f1\text{–}3} =$ 549, 606, 686 Hz) are in the upper part of the frequency range, in which the naturally growing disturbances are observed. Below, this is referred to as the main (f_m) case. In the following, the fundamental mode frequencies are chosen to cover the entire frequency range, in which the naturally arising disturbances were observed. Therefore, the frequency spacing between the fundamental modes was doubled, that is the fundamental mode frequencies are $f_{f1} = 412$ Hz, $f_{f2} = 526$ Hz and $f_{f3} = 686$ Hz. Below, this is referred to as the extended f_e frequency case.

At first, figure 30 shows the spectral disturbance evolution in the f_e case for a roughness height of $h/\delta_{1,ref} = 0.3$ (see figure 11 for the f_m case). The following observations for the f_e case are in good agreement with findings in the main frequency case: in the near wake the fundamental mode growth is most distinct, whereas further downstream a distinct growth of primary wave interaction modes at f_Δ frequencies can be observed. Secondary wave interactions $f_{f,\Delta}$ between the primary f_Δ and fundamental modes are present in a low frequency range ($f < 400$ Hz), whereas these modes cannot be found for higher frequencies ($f > 400$ Hz). Moreover, no growth is seen in the $f_{\Delta,\Delta}$ mode frequency bands indicating that there are no relevant self-interactions between the primary (f_Δ) wave interaction modes. Hence, the qualitative disturbance evolution is very similar in the f_m and f_e case. In addition, the f_e case reveals that the low frequency interaction modes can grow in a broad frequency range ($0 < f < 300$ Hz) in the roughness wake.

Figure 30(*b*) shows a detailed amplitude evolution for the fundamental modes in the f_e case at $h/\delta_{1,ref} = 0.3$ in comparison to the reference case ($h/\delta_{1,ref} = 0$). In the near wake, the growth of the fundamental modes is increased with the frequency confirming the finding in the f_m case, according to which the fundamental mode growth is weakly dependent on the fundamental mode frequency. This weak dependence might be attributed to the nonlinear initiation of the (oblique) fundamental modes by the roughness. In compliance with literature (Wang 2004), the growth is most distinct for modes near the upper branch of the neutral curve at the roughness position. In the far wake, it is seen that the growth rates of the fundamental modes match with the reference case in compliance with the f_m case. Hence, opposed to the near wake the low-frequency fundamental modes are more pronounced in the far wake.

Below, a comparison of the fundamental mode spanwise disturbance evolution is depicted in figure 31 for the f_m and f_e case. In both cases similar spanwise structures are present in a wedge-shaped region downstream of the roughness. Hence, the spanwise disturbance evolution appears rather independent of the fundamental mode frequency (within the investigated frequency range), as also hinted at in figure 9(*b*). In the f_e case the most distinct spanwise modes are, therefore, also observed near $\beta d_r = 2\pi$ (not shown). A similar tendency was observed by Wang (2004). He reported a wave propagation angle near $\Theta = 45°$ for the most distinct spanwise modes of a fundamental mode located in the upper branch region. The present investigation reveals wave propagation angles for the most dominant modes of $\Theta = 37°$ for the highest-frequency fundamental mode $f_{f3} = 686$ Hz and $\Theta = 49°$ for the lowest frequency fundamental mode $f_{f1} = 412$ Hz. Hence, taking into account the linear

https://doi.org/10.1017/jfm.2014.499 Published online by Cambridge University Press

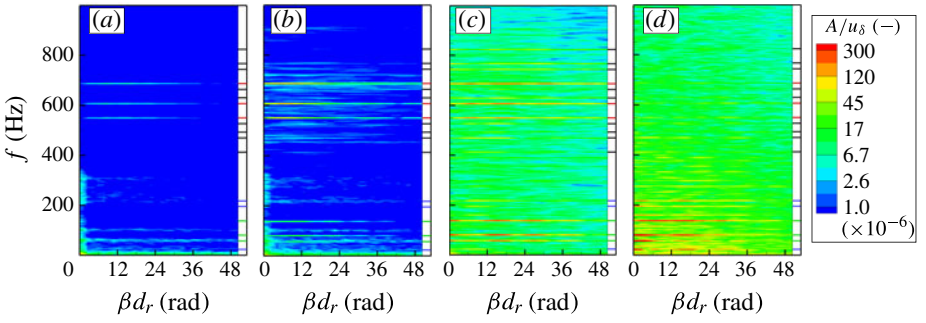


FIGURE 28. Averaged (with respect to $\pm\beta$) spanwise wavenumber spectra for $h/\delta_{1,ref} = 0.5$ at $y/\delta_{1,ref} = 1.0$ and $s/d_r = 0.75$ (a), $s/d_r = 3.75$ (b), $s/d_r = 6.75$ (c) and $s/d_r = 9.75$ (d), with frequencies of f_f, f_Δ, $f_{\Delta,\Delta}$ and $f_{f,\Delta}$ indicated on the right-hand side by red, green, blue and black lines, respectively.

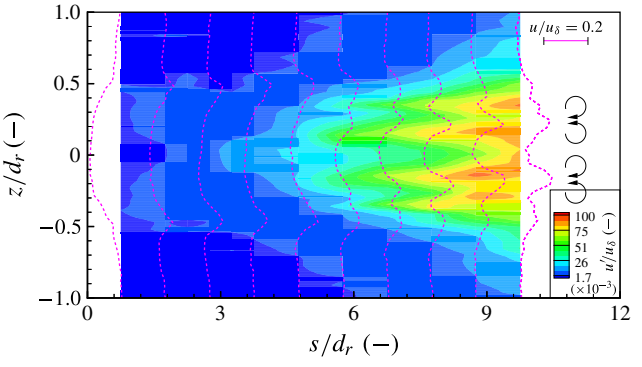


FIGURE 29. Streamwise evolution of the mean flow (dashed purple line) and of the streamwise velocity fluctuations (u' for $f = 10$–5000 Hz, coloured contours) for $h/\delta_{1,ref} = 0.5$ at $y/\delta_{1,ref} = 1.0$ (with excited fundamental modes $f_{f1\text{–}3}$).

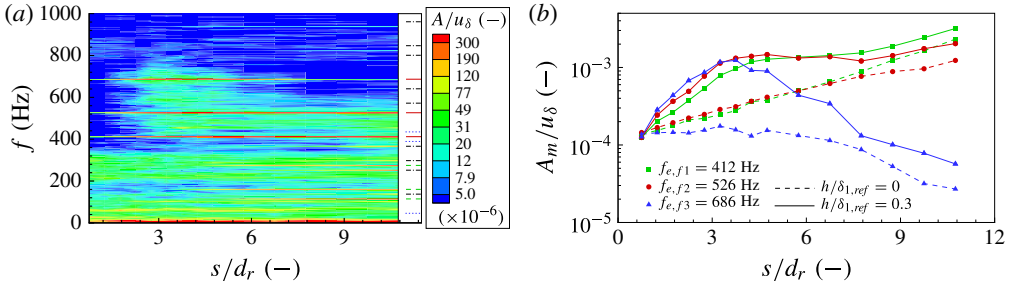


FIGURE 30. Spectral disturbance evolution (A at $y/\delta_{1,ref} = 0.9$, with frequencies of f_f, f_Δ, $f_{\Delta,\Delta}$ and $f_{f,\Delta}$ indicated by solid (red), dashed (green), dotted (blue) and dash-dot (black) lines, respectively) for $h/\delta_{1,ref} = 0.3$ (a) and amplitude evolution of fundamental modes (b) on the roughness centreline for f_e case.

https://doi.org/10.1017/jfm.2014.499 Published online by Cambridge University Press

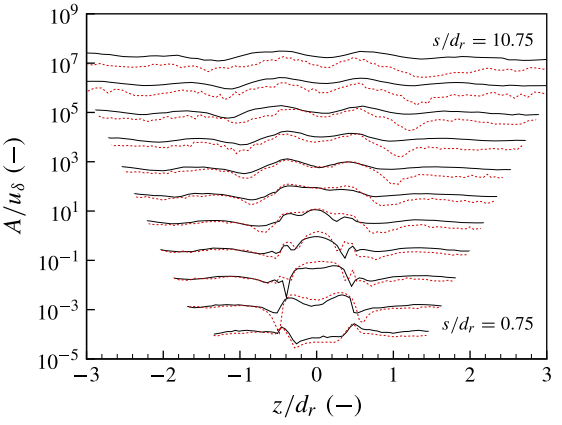


FIGURE 31. (Colour online) Evolution of fundamental mode f_{f1} in the streamwise–spanwise plane (shifted by one decade per $\Delta s/d_r = 1$) at $y/\delta_{1,ref} = 0.9$ for $h/\delta_{1,ref} = 0.3$ with $f_{m,f1} = 549$ Hz (dashed, red online) and $f_{e,f1} = 412$ Hz (solid, black).

stability characteristics of the fundamental modes in the present case (compare figure 3) reasonably good agreement with literature is seen.

In a next step, the evolution of the primary (f_Δ) interaction modes in the f_e case is discussed in figure 32 in connection with the phase speeds of the corresponding fundamental and f_Δ modes at $s/d_r = 8.75$. The spanwise wavenumber spectra, which are exemplarily shown for the $f_{m,\Delta 31} = 137$ Hz and the $f_{e,\Delta 31} = 274$ Hz mode, are normalized by the respective maximum amplitude for better comparison. It is seen that the spanwise wavenumber spectra correlate well for $\beta d_r < 8$ and that the most dominant spanwise modes are observed near $\beta d_r = 2\pi$ independent of the f_Δ disturbance frequency. The phase speeds of the two-dimensional $f_{e,f3}$ mode and the oblique $f_{e,f1}$ modes are equal near $\beta d_r = 5$. The mismatch in the phase speed of the two-dimensional $f_{e,f3}$ mode and the oblique $f_{e,f1}$ mode at a spanwise wavenumber, which is associated with the maximum in the spanwise wavenumber spectrum of the primary ($f_{e,\Delta 31}$) wave interaction mode, is 2 %. Moreover, the phase speed of the $f_{e,\Delta 31}$ mode is very similar in this spanwise wavenumber range. Hence, the phase-locked interaction mechanism can account for the growth of primary (f_Δ) interaction modes also at higher difference frequencies (f_e case) compared with the f_m case. Based on these observations one can conclude that, at first, distinct spanwise modes are prescribed by the disturbance interaction with the roughness element. Within the range of the naturally (without controlled disturbance excitation) arising disturbances in the near roughness wake ($400 < f < 750$ Hz), two-dimensional modes and (by the roughness excited) oblique modes can share approximately the same phase speeds. Therefore, a rapid (nonlinear) growth of low-frequency (f_Δ) interaction modes in the far roughness wake is present in a wide frequency range ($0 < f < 350$ Hz), most probably due to phase-locked wave interactions.

Finally, the influence of the fundamental mode frequency on the disturbance growth in the roughness wake is summarized in figure 33 for selected roughness heights in the medium height range, in particular $h/\delta_{1,ref} = [0.3, 0.4, 0.5]$. The amplitude in figure 33(*a–c*) is normalized by the amplitude of the fundamental modes at $s/d_r = 0.75$ for $h/\delta_{1,ref} = 0$ (A_f). In the near wake the growth of the fundamental modes is more distinct in the f_m case, since the fundamental modes are closer to the second branch

https://doi.org/10.1017/jfm.2014.499 Published online by Cambridge University Press

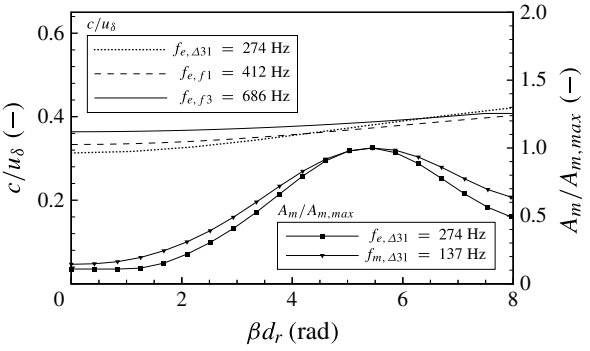


FIGURE 32. Phase speeds calculated with linear theory for $f_{e,f1}$, $f_{e,f3}$ and $f_{e,\Delta 31}$ mode and spanwise wavenumber spectrum of $f_{e,\Delta 31}$ and $f_{m,\Delta 31}$ mode for $h/\delta_{1,ref} = 0.3$ at $s/d_r = 8.75$ and $y/\delta_{1,ref} = 0.9$.

of the neutral curve (compare figure 30). In contrast, far downstream the growth is more distinct in the f_e case, in compliance with the evolution in the reference case ($h/\delta_{1,ref} = 0$). In the context of figure 25 it was found that the growth of the f_Δ modes in the near wake can be associated with a quadratic wave interaction between the respective fundamental modes. Therefore, a higher amplitude of the f_Δ interaction modes in the f_m case (compared with the f_e case, figure 33*b*) is in good agreement with the increased growth of the fundamental modes in the near wake for the f_m case. In the context of figure 33(*b*), it might be noted that the initial amplitudes ($s/d_r < 2$) reflect the noise level, which is slightly higher in the f_m case since the f_Δ modes are located in a lower-frequency range, which is stronger affected by background noise (compare e.g. figure 8*a*). In agreement with the evolution in figure 33(*a*,*b*), the overall disturbance level of the boundary layer is also increased in the f_m case, especially in the far wake (figure 33*c*). Only for $h/\delta_{1,ref} = 0.3$, the overall disturbance level is higher in the f_e case far downstream. That is because the disturbance evolution is dominated by the fundamental modes in the far wake, since the growth of the interaction modes is weaker for $h/\delta_{1,ref} = 0.3$ (compare also figure 18). In conclusion one finds that the disturbance evolution in the far wake is substantially influenced by the initial amplification of the fundamental modes. The growth rates of fundamental modes in the near wake are, in turn, highly dependent on the particular roughness height and weakly affected by the disturbance frequency in the investigated frequency range of fundamental modes, that is $f = 400$–700 Hz.

3.6. *The influence of pressure gradient*

The highest efficiency of wind turbines is obtained when operated near the upper edge of the low-drag bucket of the airfoil polar, that is at best glide ratio. Typically, with increasing blade angle the flow in the leading edge region changes from an accelerated to a decelerated state. In order to quantify the influence of this effect on the disturbance roughness interaction, three characteristic pressure distributions, that is FPG, ZPG and APG boundary layer in the airfoil leading edge region are investigated (compare figure 2*a*). Fundamental modes with the same frequencies ($f_{f1} = 549$ Hz, $f_{f2} = 606$ Hz and $f_{f3} = 686$ Hz, f_m case) as discussed in the preceding sections were excited upstream of the roughness. The RMS amplitude of the fundamental modes was adjusted to $A_m/u_\infty = 0.02\,\%$, respectively, resulting in a total RMS amplitude

https://doi.org/10.1017/jfm.2014.499 Published online by Cambridge University Press

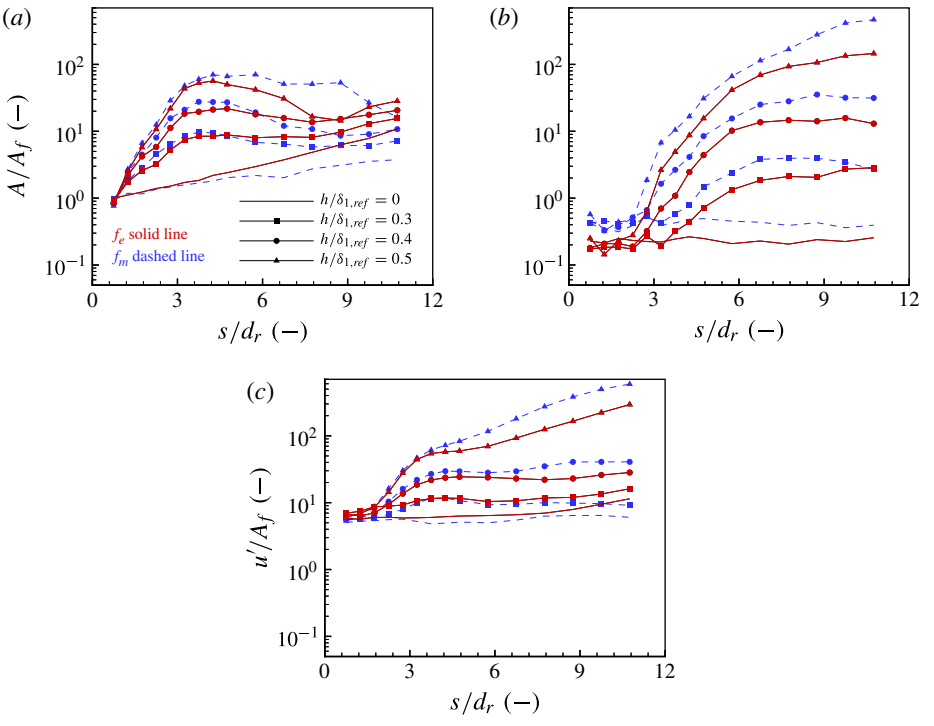


FIGURE 33. (Colour online) Disturbance evolution in f_e (solid, red online) and f_m (dashed, blue online) case for fundamental modes Σf_f (*a*), Σf_Δ modes (*b*) and integral u' velocity fluctuations (*c*), amplitude A is normalized by A_f, which is the amplitude of the fundamental modes at $s/d_r = 0.75$ for $h/\delta_{1,ref} = 0$, same legend for (*a–c*).

of the three excited fundamental modes of $A_m/u_\infty \approx 0.035\,\%$ at the position of the roughness independent of the particular pressure gradient in the leading edge region. Small differences in the amplitude at the roughness position for the different test cases are accounted for by a normalization to A_f, which is the amplitude of the fundamental modes at $s/d_r = 0.75$ for $h/\delta_{1,ref} = 0$ and the respective pressure gradient.

At first, figure 34 shows the influence of the pressure gradient on the most distinct disturbance modes, which arise in the roughness wake, that is fundamental (f_f), primary wave interaction (f_Δ) and secondary wave interaction ($f_{f,\Delta}$ and $f_{\Delta,\Delta}$) modes. The roughness height is adjusted to $h/\delta_{1,ref} = 0.5$ taking into account the growing displacement thickness at the roughness position with increasing pressure gradient (compare also table 1). In the near wake of the roughness ($s/d_r < 4$) the fundamental mode amplitude turns out to be only very weakly dependent on the pressure gradient (figure 34*a*). In the FPG case the amplitude maximum near $s/d_r = 4$ is slightly lower compared with the ZPG and APG case. Further downstream ($s/d_r > 4$) the fundamental modes are damped in the FPG case, whereas in the ZPG and APG case the amplitude remains at a nearly constant level, at first, before being slightly damped. In the near-wake evolution of the primary interaction modes (figure 34*b*), the growth is also slightly smaller in the FPG case and further downstream ($s/d_r > 6$) the growth in the ZPG and APG case is considerably more distinct compared with the FPG case. Based on linear theory f_Δ modes are stable in the entire measurement domain also for the FPG and APG case, that is in the APG case modes with $f < 150$ Hz

https://doi.org/10.1017/jfm.2014.499 Published online by Cambridge University Press

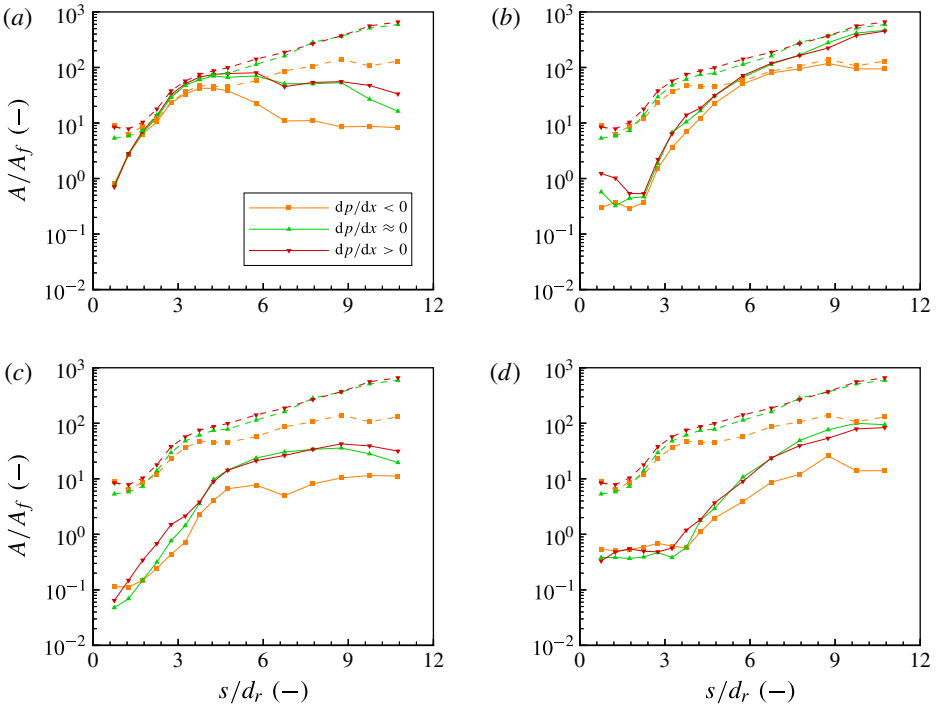


FIGURE 34. (Colour online) Disturbance evolution on roughness centreline depending on pressure gradient for $h/\delta_{1,ref} = 0.5$, Σf_f mode (*a*), Σf_Δ mode (*b*), $\Sigma f_{f,\Delta}$ mode (*c*) and $\Sigma f_{\Delta,\Delta}$ mode (*d*), integral streamwise velocity fluctuations (u' for $f = 10$–5000 Hz) indicated with dashed lines, amplitude A is normalized by A_f, which is the amplitude of the fundamental modes at $s/d_r = 0.75$ for $h/\delta_{1,ref} = 0$ and the respective pressure gradient, same legend for (*a–d*).

are stable. Therefore, in compliance with previous findings concerning the influence of the roughness height (§ 3.4) and the disturbance frequency (§ 3.5), it is observed that a rather weak difference in the initial growth of the fundamental modes in the near roughness wake has a great impact on the disturbance evolution in the far wake. This conclusion is further corroborated by the evolution of the secondary interaction modes ($f_{f,\Delta}$ and $f_{\Delta,\Delta}$), which is very similar in the ZPG and APG case, whereas the disturbance growth is less pronounced for the FPG case especially in the far wake. Finally, a comparison with the overall disturbance level of the boundary layer (indicated with dashed lines) shows that the fundamental modes dominate the growth in the near wake, whereas the low-frequency interaction (f_Δ) modes prevail in the far wake independent of the particular pressure gradient.

The preceding discussion showed that for a roughness height of $h/\delta_{1,ref} = 0.5$, no considerable influence of the pressure gradient was present in the ZPG and APG case. Comparing the overall disturbance evolution (figure 34*d*) of the boundary layer in the APG and ZPG case indicates that turbulence is already triggered by the rapid disturbance growth in the ZPG case (compare also figures 27 and 28). Hence, an increase in pressure gradient hardly affects the streamwise disturbance evolution and, therewith, the onset of turbulence. In contrast, in the FPG case the lower disturbance growth suggests that the onset of turbulence is delayed with decreasing pressure

https://doi.org/10.1017/jfm.2014.499 Published online by Cambridge University Press

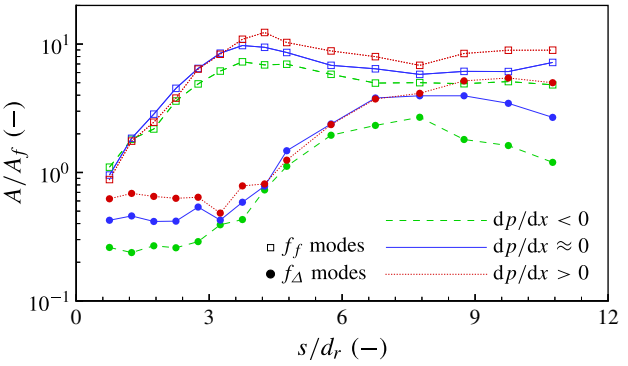


FIGURE 35. (Colour online) Disturbance evolution of fundamental (Σf_f) modes and Σf_Δ modes on roughness centreline for $h/\delta_{1,ref} = 0.3$, amplitude A is normalized by A_f, which is the amplitude of the fundamental modes at $s/d_r = 0.75$ for $h/\delta_{1,ref} = 0$ and the respective pressure gradient.

gradient. In this context, figure 35 depicts the disturbance evolution on the roughness centreline for the fundamental and the primary interaction (f_Δ) modes at a lower roughness height of $h/\delta_{1,ref} = 0.3$. In the near wake the fundamental mode growth is slightly more distinct and, consequently, the maximum near $s/d_r = 4$ is more pronounced with increasing pressure gradient. Further downstream, the evolution of the fundamental modes is similar, despite the amplitude being increased with the pressure gradient. Consequently, the growth of the primary interaction modes differs in the far roughness wake. In the APG case, the f_Δ mode growth levels off with the stabilization of the mean flow, whereas the interaction modes are considerably damped in the ZPG and the FPG case. Therefore, if the onset of turbulence is not triggered immediately by the disturbance growth in the near wake, a decreasing pressure gradient results in a less distinct growth of the fundamental and the subsequent interaction modes in the wake of medium height roughness elements.

In the above-discussed results the amplitude of the disturbance modes was adjusted equally, that is independent of the pressure gradient. However, in the natural (without controlled disturbance excitation) case, the disturbance level of the laminar boundary layer depends on the pressure gradient, especially in the leading edge region, in which the roughness is located. Therefore, the disturbance roughness interaction involves different incoming disturbance amplitude levels with changing pressure gradient. Hence, the effect of pressure gradient on the disturbance evolution in the roughness wake might even be more pronounced in the natural case compared with the experiments with controlled disturbance excitation. Figure 36 depicts the disturbance evolution in the natural case for a roughness height of $h/\delta_{1,ref} = 0.5$. The disturbance evolution is evaluated in particular frequency bands that is low (f = 100–200 Hz, figure 36*a*), medium (f = 350–450 Hz, figure 36*b*) and high (f = 650–750 Hz, figure 36*c*). At the roughness position, the natural disturbance amplitudes are below the signal-to-noise ratio for all cases (FPG–APG) due to the very low turbulence level of the LWT. Hence, the disturbance evolution can only be studied in the roughness wake.

In the favourable pressure gradient case, a substantial disturbance growth can only be observed close to the roughness in the high-frequency band. However, in the streamwise evolution the high-frequency disturbances are damped with the

https://doi.org/10.1017/jfm.2014.499 Published online by Cambridge University Press

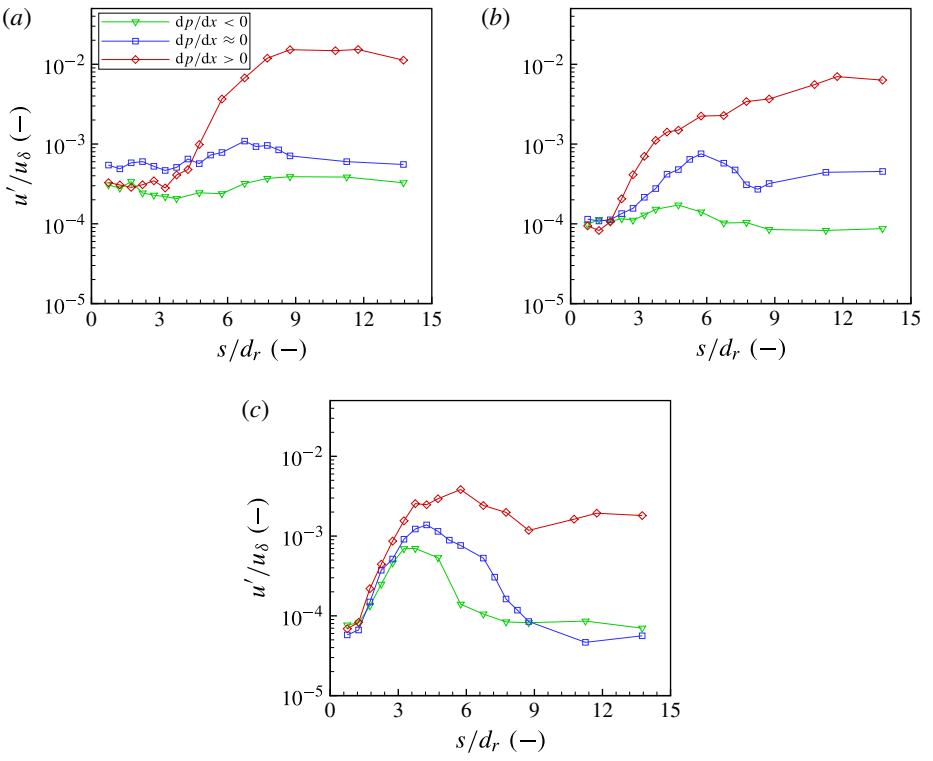


FIGURE 36. (Colour online) Disturbance evolution on roughness centreline in unperturbed (without disturbance excitation) case for $h/\delta_{1,ref} = 0.5$, low-frequency ($f = 100$–200 Hz) (a), medium-frequency ($f = 350$–450 Hz) (b) and high-frequency ($f = 650$–750 Hz) (c) disturbance band, same legend for (a–c).

stabilization of the mean flow. Therefore, in the FPG case the disturbance roughness interaction does not affect the evolution of the laminar boundary layer within the measurement domain ($s/d_r < 14$). In the ZPG case, the disturbance amplitudes in the high-frequency band are more distinct (compared with the FPG case) and a disturbance growth can also be observed in the medium-frequency band. The increased disturbance amplitudes in the medium- and high-frequency band in the near roughness wake involve a very weak growth of low-frequency modes for $s/d_r > 6$. In the APG case a further increased disturbance growth in the medium- and high-frequency band results in a rapid amplification of low-frequency modes. It is seen that the low-frequency modes dominate the disturbance growth for $s/d_r > 6$ and finally trip turbulence (compare also figure 6). Comparing the disturbance evolution in the near roughness wake (high-frequency band, figure 36c) shows that the pressure gradient substantially influences the disturbance amplification, whereas the impact on the initial natural disturbance amplitudes at the roughness position seems to be of second-order importance in the present case. However, one has to keep in mind that the turbulence level of the LWT is extremely low and, therefore, also the disturbance amplitudes of the laminar boundary layer at the roughness position.

Finally, the results obtained with controlled disturbance excitation compare well with the disturbance growth in the natural case with regard to the following findings: the disturbance growth in the near wake is most pronounced for modes near the

https://doi.org/10.1017/jfm.2014.499 Published online by Cambridge University Press

upper branch of the neutral curve at the roughness position, whereas these modes are considerably damped with the relaxation of the mean flow for $s/d_r > 4$. The growth of the high-frequency modes in the near wake involves a nonlinear growth of low-frequency (interaction) modes in the far wake. In case the high-frequency modes gain a high enough amplitude, the low-frequency modes overtake and are dominant in the far roughness wake. Hence, the investigations of controlled and natural disturbance interactions with the roughness reveal that the growth of high-frequency modes in the near wake can initiate a nonlinear growth of low-frequency interaction modes, which is regarded the key mechanism for tripping turbulence in the far wake of medium height roughness elements.

4. Conclusion

The disturbance evolution downstream of a single, cylindrical roughness element has been experimentally investigated using hot-wire anemometry. The roughness element is placed in a laminar boundary layer in an airfoil leading edge region. The disturbance evolution in the roughness wake has been studied under natural and controlled disturbance conditions. In the natural case the initial disturbance level at the roughness was determined by the very low background noise level of the wind tunnel flow. In the controlled case, TS waves have been excited upstream of the roughness element by perturbing the laminar boundary layer with wall-normal suction and blowing. The influence of the following parameters on the disturbance evolution has been addressed: height of the roughness element, frequency and amplitude of the disturbance modes and stability characteristics due to different pressure gradients.

In the natural case the mean flow and the disturbance evolution of the laminar boundary layer are only weakly affected for low height roughness elements ($h/\delta_{1,ref} < 0.2$). In the medium height range ($0.2 < h/\delta_{1,ref} < 0.5$) high- and low-speed streaks indicate the presence of two counter-rotating vortex pairs in the near roughness wake in agreement with findings by Délery (2001). In the streamwise evolution a damping of the vortical structures results in a relaxation of the boundary layer mean flow towards a spanwise uniform state. Hence, far downstream the shape factor approaches the undisturbed reference case. In contrast, for high elements ($h/\delta_{1,ref} > 0.75$) the disturbance growth in the roughness wake trips turbulence, before the mean flow can recover from the roughness interaction. The roughness Reynolds number in this case is $R_h = 445$, which is in good agreement with previous findings for a cylindrical roughness element (Gregory & Walker 1956; Klebanoff *et al.* 1992).

The main experiments focus on the medium roughness height range. In the near wake the most dominant disturbance growth is observed for modes, which show the highest amplitudes at the roughness according to linear stability theory. Further downstream these modes are, however, considerably damped with the relaxation of the mean flow, whereas a continuous growth of low-frequency modes is observed. This characteristic evolution in the natural case, which is associated with a low initial disturbance level at the roughness, was studied in detail by controlled disturbance excitation upstream of the roughness.

Controlled low-amplitude ($A/u_\infty = 0.035\,\%$ at the roughness position), two-dimensional fundamental TS modes (f_f) were excited in the frequency range of the naturally arising disturbances observed in the near roughness wake. Immediately downstream of the roughness a nonlinear growth of these fundamental modes is present. The growth is more pronounced for higher-frequency modes, that is modes, which are closer to the second branch of the neutral curve in compliance with

https://doi.org/10.1017/jfm.2014.499 Published online by Cambridge University Press

observations by Wang (2004). The excess (compared with linear theory) growth of the initially two-dimensional TS modes in the near wake is accompanied by the formation of oblique modes, which are most distinct close to the critical layer. The wavelength of the most pronounced spanwise modes is of the order of the roughness diameter and of the streamwise wavelength of the fundamental modes. Consequently, the corresponding wave propagation angles are close to $\Theta = 45°$. In the streamwise evolution the oblique fundamental modes are damped with the relaxation of the mean flow towards a spanwise uniform state. Therefore, far downstream the fundamental mode energy is predominately contained in the two-dimensional modes in agreement with previous findings by de Paula *et al.* (2008) and the growth rates of the fundamental modes match with the linear growth rates present in the undisturbed reference case ($h/\delta_{1,ref} = 0$).

The nonlinear growth of the fundamental modes in the near roughness wake results in interactions in between the fundamental modes. Hence, additional modes at sum and difference frequencies develop. The sum modes are only weakly pronounced and their growth is explained by a quadratic wave interaction of the fundamental modes. In contrast, the f_Δ difference modes are significantly more distinct. In a first stage their growth can also be attributed to the quadratic wave interaction of the fundamental modes. Further downstream, the nonlinear growth of the f_Δ modes is associated with phase-locked interactions between the two-dimensional fundamental modes and by the roughness excited oblique fundamental modes, which share approximately the same phase speed (Wu *et al.* 2007). Hence, opposed to the fundamental mode evolution, the spanwise structures of the f_Δ modes rise despite the mean flow relaxation in the far wake. In this second weakly nonlinear growth stage the shape of the f_Δ mode complies, however, still with linear theory similar as observed in the experiments by de Paula *et al.* (2013).

The disturbance evolution in the roughness wake further reveals secondary wave interactions, which are most distinct between the fundamental f_f and the f_Δ modes. Similar as observed for the primary f_Δ combination modes the secondary $f_{f,\Delta}$ modes have a highly three-dimensional nature. The growth rates of the secondary interaction modes are higher compared with linear theory or to a quadratic interaction of the respective fundamental and primary wave interaction modes. Similar phase speeds of the two-dimensional fundamental and the oblique f_Δ modes, which are associated with the respective secondary interaction mode, suggest that the nonlinear growth of the secondary ($f_{f,\Delta}$) modes can also be attributed to phase-locked wave interactions.

Within the medium roughness height range the disturbance growth substantially depends on the particular roughness height. For $h/\delta_{1,ref} = 0.2$ the disturbance growth is dominated by the fundamental mode evolution, whereas interaction modes are only very weakly pronounced. The amplification of the fundamental modes in the near wake increases considerably with the roughness height and, consequently, the growth of the interaction modes. For $h/\delta_{1,ref} > 0.3$, self-interactions in between the primary f_Δ modes occur and the modal shape of the f_Δ modes starts to deform in the process of transition. This seems to represent a fully interactive growth stage, that follows the initial stage of phase-locked interactions. Finally, tertiary wave interaction become obvious. As a consequence, the disturbance spectrum progressively fills up resulting in a broadband character, that can be associated with the onset of turbulence.

The growth of the low-frequency (f_Δ) modes is in the first two stages associated with a quadratic and a phase-locked interaction in between the fundamental modes, respectively. Therefore, the growth of the low-frequency modes highly depends on the initial growth of the fundamental modes in the near roughness wake. The initial

https://doi.org/10.1017/jfm.2014.499 Published online by Cambridge University Press

growth of the fundamental modes, in turn, is weakly dependent on the fundamental mode frequency, whereas the amplification rates are considerably increasing with the pressure gradient. The most significant parameter for the initial growth of the fundamental modes is, however, the mean flow distortion in the near wake, that is the roughness height. In agreement with the disturbance evolution in the natural (without controlled disturbance excitation) case it is seen that the low-frequency (f_Δ) interaction modes dominate the disturbance evolution in the far wake, if the initial growth of the fundamental modes in the near roughness wake is strong enough for nonlinear interactions to occur.

Acknowledgement

This work is supported by DFG (Deutsche Forschungsgemeinschaft) under grant WU265/4-1.

REFERENCES

ACARLAR, M. & SMITH, C. 1987 A study of hairpin vortices in a laminar boundary-layer. Part 1. Hairpin vortices generated by a hemisphere protuberance. *J. Fluid Mech.* **175**, 1–41.

AIZIN, L. B. & POLYAKOV, N. F. 1979 Acoustic generation of Tollmien–Schlichting waves over local unevenness of surfaces immersed in streams. Preprint 17, *Akad. Nauk USSR*, Siberian Div., Institute of Theoretical and Applied Mechanics, Novosibirsk.

ANDERSSON, P., BRANDT, L., BOTTARO, A. & HENNINGSON, D. S. 2001 On the breakdown of boundary layer streaks. *J. Fluid Mech.* **428**, 29–60.

BAKCHINOV, A. A., GREK, G. R., KLINGMANN, B. G. B. & KOZLOV, V. V. 1995 Transition experiments in a boundary layer with embedded streamwise vortices. *Phys. Fluids* **7**, 820–832.

BORODULIN, V. I., KACHANOV, Y. S. & KOPTSEV, D. 2002*a* Experimental study of resonant interactions of instability waves in a self-similar boundary layer with an adverse pressure gradient: III. Broadband disturbances. *J. Turbul.* **3** (64), 1–19.

BORODULIN, V. I., KACHANOV, Y. S., KOPTSEV, D. & RESCHEKTAYEV, A. P. 2002*b* Experimental study of resonant interactions of instability waves in a self-similar boundary layer with an adverse pressure gradient: II. Detuned resonance. *J. Turbul.* **3** (63), 1–32.

BREUER, K. S., COHEN, J. & HARITONIDIS, J. H. 1997 The late stages of transition induced by a low-amplitude wavepacket in a laminar boundary layer. *J. Fluid Mech.* **340**, 395–411.

CEBECI, T. & EGAN, D. A. 1989 Prediction of transition due to isolated roughness. *AIAA J.* **27** (7), 870–875.

CEBECI, T. & SMITH, A. M. O. 1974 *Analysis of Turbulent Boundary Layers*. Academic Press.

CHOUDHARI, M. & KERSCHEN, E. J. 1990 Instability wave patterns generated by interaction of sound waves with three-dimensional wall suction or roughness. *AIAA Paper* 90-119.

CONTE, S. 1966 The numerical solution of linear boundary layer value problems. *SIAM Rev.* **8** (3), 309–321.

CORKE, T. C. & MANGANO, R. A. 1989 Resonant growth of three-dimensional modes in transitioning Blasius boundary layers. *J. Fluid Mech.* **209**, 93–150.

COSSU, C. & BRANDT, L. 2002 Stabilization of Tollmien–Schlichting waves by finite amplitude optimal streaks in the Blasius boundary layer. *Phys. Fluids* **14**, 57–60.

COSSU, C. & BRANDT, L. 2004 On Tollmien–Schlichting-like waves in streaky boundary layers. *Eur. J. Mech. (*B*/Fluids)* **23**, 815–833.

CROUCH, J. D. 1997 Excitation of secondary instabilities in boundary layers. *J. Fluid Mech.* **336**, 245–266.

CROUCH, J. D., KOSORYGIN, V. S. & NG, L. L. 2006 Modeling the effects of steps on boundary-layer transition. In *6th IUTAM Symposium on Laminar–Turbulent Transition* (ed. R. Govindarajan), pp. 37–44. Springer.

https://doi.org/10.1017/jfm.2014.499 Published online by Cambridge University Press

DÉLERY, J. M. 2001 R. Legendre and H. Werle: toward the elucidation of three-dimensional separation. *Annu. Rev. Fluid Mech.* **33**, 129–154.

VON DOENHOFF, A. E. & BRASLOW, A. L. 1961 The effect of distributed surface roughness on laminar flow. *Boundary Layer Flow Control* **2**, 657–681.

DOVGAL, A. V. & KOZLOV, V. V. 1990 Hydrodynamic instability and receptivity of small scale separation regions. In *IUTAM Symposium on Laminar–Turbulent Transition* (ed. D. Arnal & R. Michel), pp. 523–531. Springer.

DRELA, M. 1989 XFoil: An analysis and design system for low Reynolds number airfoils. In *Low Reynolds Number Aerodynamics* (ed. T. J. Mueller), Lecture Notes in Engineering, vol. 54, pp. 1–12. Springer.

DRYDEN, H. L. 1953 Review of published data on the effect of roughness on transition from laminar to turbulent flow. *J. Aeronaut. Sci.* 477–482.

ERGIN, F. G. & WHITE, E. B. 2006 Unsteady and transitional flows behind roughness elements. *AIAA J.* **44** (11), 2504–2514.

FAGE, A. 1943 The smallest size of a spanwise surface corrugation which affects boundary layer transition on an aerofoil. Aeronautical Research Council, Reports and Memoranda (2120).

FOKEN, T. 2006 *Angewandte Meteorologie*. Springer.

FRANSSON, J. H. M., BRANDT, L., TALAMELLI, A. & COSSU, C. 2004 Experimental and theoretical investigation of the nonmodal growth of steady streaks in flat plate boundary layer. *Phys. Fluids* **16**, 3627–3638.

FRANSSON, J. H. M., BRANDT, L., TALAMELLI, A. & COSSU, C. 2005 Experimental study of the stabilization of Tollmien–Schlichting waves by finite amplitude streaks. *Phys. Fluids* **17**, 054110.

GASTER, M., GROSCH, C. E. & JACKSON, T. L. 1994 Velocity field created by a shallow bump in a boundary layer. *Phys. Fluids* **6**, 2104–3079.

GOLDSTEIN, M. E. 1985 Scattering of sound waves into Tollmien–Schlichting waves by small streamwise variations in surface geometry. *J. Fluid Mech.* **154**, 509–529.

GREGORY, N. & WALKER, W. S. 1956 The effect on transition of isolated surface excrescences in the boundary layer. Aeronautical Research Council, Reports and Memoranda (2779).

HERR, STEFAN. 2004 Experimental investigation of airfoil boundary-layer receptivity and a method for the characterization of the relevant free-stream disturbances. PhD thesis, University of Stuttgart.

JACOBS, E. N. 1939 Preliminary report on laminar-flow airfoils and new methods adopted for airfoil and boundary-layer investigations. *Tech. Rep.* 345. NACA WR L.

KACHANOV, Y. S. 1994 Physical mechanisms of laminar boundary-layer transition. *Annu. Rev. Fluid Mech.* **26**, 411–482.

KACHANOV, Y. S. 2000 Three-dimensional receptivity of boundary layers. *Eur. J. Mech. (*B*/Fluids)* **19**, 723–744.

KENDALL, J. M. 1981 Laminar boundary layer velocity distortion by surface roughness: effect upon stability. *AIAA Paper* 1981-0195.

KLEBANOFF, P. S., CLEVELAND, W. G. & TIDSTROM, K. D. 1992 On the evolution of a turbulent boundary-layer induced by a three-dimensional roughness element. *J. Fluid Mech.* **237**, 101–187.

KLEBANOFF, P. S. & TIDSTROM, K. D. 1972 Mechanism by which a two-dimensional roughness element induces boundary-layer transition. *Phys. Fluids* **15** (17), 1173–1188.

LANDAHL, M. T. 1980 A note on an algebraic instability of inviscid parallel shear flows. *J. Fluid Mech.* **98**, 243–251.

MASAD, J. A. & LYER, V. 1994 Transition prediction and control in subsonic flow over hump. *Phys. Fluids* **6**, 313–327.

MATHEIS, B. D., HUEBSCH, W. W. & ROTHMAYER, A. P. 2004 Separation and unsteady vortex shedding from leading edge surface roughness. Paper published in RTO-MP-AVT-111.

MOCHIZUKI, M. 1961*a* Hot wire investigations of smoke patterns caused by a spherical roughness element. *Nat. Sci. Rep. Ochanomizu Univ.* **12** (2), 87–101.

https://doi.org/10.1017/jfm.2014.499 Published online by Cambridge University Press

MOCHIZUKI, M. 1961*b* Smoke observation on boundary layer transition caused by a spherical roughness element. *J. Phys. Soc. Japan* **16**, 995–1008.

MORKOVIN, M. V. 1990 On roughness-induced transition: facts, views and speculations. In *Instability and Transition* (ed. M. Y. Hussaini & R. G. Voigt), vol. 1, pp. 281–295. Springer.

NAYFEH, A. H., RAGAB, S. A. & AL-MAAITAH, A. 1988 Effect of bulges on the stability of boundary layers. *Phys. Fluids* **31**, 796–806.

DE PAULA, I. B., WÜRZ, W., KRÄMER, E., BORODULIN, V. I. & KACHANOV, Y. S. 2010 Generation of seeds of subharmonic resonance in an airfoil boundary-layer transition initiated by modulated TS waves. *International Conference on Methods of Aerophysical Research,* Novosibirsk.

DE PAULA, I. B., WÜRZ, W., KRÄMER, E., BORODULIN, V. I. & KACHANOV, Y. S. 2013 Weakly non-linear stages of boundary-layer transition initiated by modulated Tollmien–Schlichting waves. *J. Fluid Mech.* **732**, 571–615.

DE PAULA, I. B., WÜRZ, W. & MEDEIROS, M. A. F. 2008 Experimental study of a Tollmien–Schlichting wave interacting with a shallow 3D roughness element. *J. Turbul.* **9**, 1–23.

PIOT, E., CASALIS, G. & RIST, U. 2008 Stability of the laminar boundary layer flow encountering a row of roughness elements: biglobal stability approach and DNS. *Eur. J. Mech. (*B*/Fluids)* **27**, 684–706.

PLOGMANN, B. & WÜRZ, W. 2013 Aeroacoustic measurements on a NACA 0012 applying the coherent particle velocity method. *Exp. Fluids* **54** (7), 1556.

PLOGMANN, B., WÜRZ, W. & KRÄMER, E. 2012*a* Interaction of a laminar boundary layer with a cylindrical roughness element near an airfoil leading edge. *42nd AIAA Fluid Dynamic Conference, New Orleans*, AIAA Paper 2012-3077.

PLOGMANN, B., WÜRZ, W. & KRÄMER, E. 2012*b* Interaction of a three-dimensional roughness element with a TS-wave near an airfoil leading edge. *16th International Conference on Methods of Aerophysical Research—ICMAR, Kazan*.

PLOGMANN, B., WÜRZ, W. & KRÄMER, E. 2014 Interaction of a cylindrical roughness element and a two-dimensional TS-wave. In *New Results in Numerical and Experimental Fluid Mechanics IX* (ed. A. Dillmann, G. Heller, E. Krämer, H. P. Kreplin, W. Nitsche & U. Rist), pp. 163–172. Springer.

RIST, U. & JÄGER, A. 2004 Unsteady disturbance generation and amplification in the boundary-layer flow behind a medium sized roughness element. In *6th IUTAM Symposium on Laminar–Turbulent Transition* (ed. R. Govindarajan), pp. 293–298. Springer.

RUBAN, A. I. 1984 On the generation of Tollmien–Schlichting waves by sound. Translated from *Izv. Akad. Nauk SSSR, Mech. Zhidk. i Gaza*, No. 5, pp. 44–52.

SARIC, W. S., REED, H. L. & KERSCHEN, E. J. 2002 Boundary-layer receptivity to freestream disturbances. *Annu. Rev. Fluid Mech.* **34**, 291–319.

SARIC, W. S., HOOS, J. A. & RADEZSKY, R. H. 1991 Boundary layer receptivity of sound with roughness. In *Boundary Layer Stability and Transition to Turbulence; Proceedings of the Symposium, ASME and JSME Joint Fluids Engineering Conference, 1st, Portland, OR, June 23–27, 1991* (ed. D. C. Reda, H. L. Reed & R. Kobayashi), pp. 17–22. American Society of Mechanical Engineers.

TADJFAR, M. & BODONYI, R. J. 1992 Receptivity of a laminar boundary layer to the interaction of a three-dimensional roughness element with time-harmonic free-stream disturbances. *J. Fluid Mech.* **242**, 701–720.

TANI, I. 1961 Effect of two-dimensional and isolated roughness on laminar flow. *Boundary Layer Flow Control Pergamon Press* **2**, 637–656.

TANI, I. 1969 Boundary-layer transition. *Annu. Rev. Fluid Mech.* **1**, 169–196.

TANI, I. & HAMA, R. 1940 On the permissible roughness in the laminar boundary layer. *Report Aeronautical Research Institute of Tokyo Imperial University* 199 pp. 419–429.

TERENTEV, E. D. 1981 Linear problem for a vibrator in subsonic boundary layer. *Prikl. Mat. Mekh.* **45**, 1049–1055.

TOBAK, M. & PEAKE, D. J. 1982 Topology of three-dimensional separated flows. *Annu. Rev. Fluid Mech.* **14**, 61–85.

https://doi.org/10.1017/jfm.2014.499 Published online by Cambridge University Press

USTINOV, M. V. 1995 Secondary instability modes generated by a Tollmien–Schlichting wave scattering from a bump. *Theor. Comput. Fluid Dyn.* **7**, 341–354.

WANG, Y. X. 2004 Instability and transition of boundary layer flows disturbed by steps and bumps. PhD thesis, Queen Mary College, University of London, UK.

WORTMANN, F. X. & ALTHAUS, D. 1964 Der Laminarwindkanal des Instituts für Aero- und Gasdynamik an der Technischen Hochschule Stuttgart. *Z. Flugwiss.* **12** (4), 129–134.

WU, X. & HOGG, L. W. 2006 Acoustic radiation of Tollmien–Schlichting waves as they undergo rapid distortion. *J. Fluid Mech.* **550**, 307–347.

WU, X. & LUO, J. 2003 Linear and nonlinear instabilities of a Blasius boundary layer perturbed by streamwise vortices. Part 1. Steady streaks. *J. Fluid Mech.* **483**, 225–248.

WU, X. & STUART, P. 1996 Interaction of phase-locked modes: a new mechanism for the rapid growth of three-dimensional disturbances. *J. Fluid Mech.* **316**, 335–372.

WU, X., STUART, P. & COWLEY, S. J. 2007 On the catalytic role of the phase-locked interaction of Tollmien–Schlichting waves in boundary layer transition. *J. Fluid Mech.* **590**, 265–294.

WÜRZ, W., HERR, S., WÖRNER, A., RIST, U., WAGNER, S. & KACHANOV, Y. S. 2003 Three-dimensional acoustic receptivity of a boundary-layer on an airfoil: experiments and direct numerical simulations. *J. Fluid Mech.* **478**, 135–163.

WÜRZ, W., SARTORIUS, D., KLOKER, M., BORODULIN, V. I., KACHANOV, Y. S. & SMORODSKY, B. V. 2012 Nonlinear instabilities of a non-self-similar boundary layer on an airfoil: experiments, DNS and theory. *Eur. J. Mech. (*B*/Fluids)* **31**, 102–128.

https://doi.org/10.1017/jfm.2014.499 Published online by Cambridge University Press